

## Validation of MIPAS HNO<sub>3</sub> operational data

D. Y. Wang<sup>1,2</sup>, M. Höpfner<sup>1</sup>, C. E. Blom<sup>1</sup>, W. E. Ward<sup>2</sup>, H. Fischer<sup>1</sup>, T. Blumenstock<sup>1</sup>, F. Hase<sup>1</sup>, C. Keim<sup>1</sup>, G. Y. Liu<sup>1</sup>, S. Mikuteit<sup>1</sup>, H. Oelhaf<sup>1</sup>, G. Wetzel<sup>1</sup>, U. Cortesi<sup>3</sup>, F. Mencaraglia<sup>3</sup>, G. Bianchini<sup>3</sup>, G. Redaelli<sup>4</sup>, M. Pirre<sup>5</sup>, V. Catoire<sup>5</sup>, N. Huret<sup>5</sup>, C. Vigouroux<sup>6</sup>, M. De Mazière<sup>6</sup>, E. Mahieu<sup>7</sup>, P. Demoulin<sup>7</sup>, S. Wood<sup>8</sup>, D. Smale<sup>8</sup>, N. Jones<sup>9</sup>, H. Nakajima<sup>10</sup>, T. Sugita<sup>10</sup>, J. Urban<sup>11</sup>, D. Murtagh<sup>11</sup>, C. D. Boone<sup>12</sup>, P. F. Bernath<sup>12,13</sup>, K. A. Walker<sup>12,14</sup>, J. Kuttippurath<sup>15,16</sup>, A. Kleinböhl<sup>15,18</sup>, G. Toon<sup>18</sup>, and C. Piccolo<sup>19</sup>

<sup>1</sup>Institut für Meteorologie und Klimaforschung (IMK), Forschungszentrum Karlsruhe und Universität Karlsruhe, Karlsruhe, Germany

<sup>2</sup>Physics Department, University of New Brunswick, Fredericton, New Brunswick, Canada

<sup>3</sup>Istituto di Fisica Applicata “N. Carrara” (IFAC) del Consiglio Nazionale delle Ricerche (CNR), Firenze, Italy

<sup>4</sup>Dipartimento di Fisica, CETEMPS, Università di L’Aquila, L’Aquila, Italy

<sup>5</sup>Laboratoire de Physique et Chimie de l’Environnement, Université d’Orléans (LPCE-CNRS), Orléans, France

<sup>6</sup>Belgian Institute for Space Aeronomy (BIRA-IASB), Brussels, Belgium

<sup>7</sup>Institut d’Astrophysique et de Géophysique, University of Liège (ULg), Liège, Belgium

<sup>8</sup>National Institute for Water and Atmospheric Research (NIWA), Lauder, Otago, New Zealand

<sup>9</sup>University of Wollongong, Wollongong, Australia

<sup>10</sup>National Institute for Environmental Studies, Tsukuba, Japan

<sup>11</sup>Department of Radio and Space Science, Chalmers University of Technology, Göteborg, Sweden

<sup>12</sup>Department of Chemistry, University of Waterloo, Waterloo, Ontario, Canada

<sup>13</sup>Department of Chemistry, University of York, Heslington, York, UK

<sup>14</sup>Department of Physics, University of Toronto, Toronto, Canada

<sup>15</sup>Institute of Environmental Physics, University of Bremen, Bremen, Germany

<sup>16</sup>CNRS/LMD Ecole Polytechnique, Palaiseau Cedex, France

<sup>18</sup>Jet Propulsion Laboratory, California Institute of Technology, Pasadena, CA, USA

<sup>19</sup>Department of Physics, Oxford University, Oxford, UK

Received: 29 March 2007 – Published in Atmos. Chem. Phys. Discuss.: 17 April 2007

Revised: 15 August 2007 – Accepted: 15 August 2007 – Published: 21 September 2007

**Abstract.** Nitric acid (HNO<sub>3</sub>) is one of the key products that are operationally retrieved by the European Space Agency (ESA) from the emission spectra measured by the Michelson Interferometer for Passive Atmospheric Sounding (MIPAS) onboard ENVISAT. The product version 4.61/4.62 for the observation period between July 2002 and March 2004 is validated by comparisons with a number of independent observations from ground-based stations, aircraft/balloon campaigns, and satellites. Individual HNO<sub>3</sub> profiles of the ESA MIPAS level-2 product show good agreement with those of MIPAS-B and MIPAS-STR (the balloon and aircraft version of MIPAS, respectively), and the balloon-borne infrared spectrometers MkIV and SPIRALE, mostly matching the reference data within the combined instrument error bars. In

most cases differences between the correlative measurement pairs are less than 1 ppbv (5–10%) throughout the entire altitude range up to about 38 km (~6 hPa), and below 0.5 ppbv (15–20% or more) above 30 km (~17 hPa). However, differences up to 4 ppbv compared to MkIV have been found at high latitudes in December 2002 in the presence of polar stratospheric clouds. The degree of consistency is further largely affected by the temporal and spatial coincidence, and differences of 2 ppbv may be observed between 22 and 26 km (~50 and 30 hPa) at high latitudes near the vortex boundary, due to large horizontal inhomogeneity of HNO<sub>3</sub>. Similar features are also observed in the mean differences of the MIPAS ESA HNO<sub>3</sub> VMRs with respect to the ground-based FTIR measurements at five stations, aircraft-based SAFIRE-A and ASUR, and the balloon campaign IBEX. The mean relative differences between the MIPAS and FTIR HNO<sub>3</sub> partial columns are within ±2%, comparable to the MIPAS

Correspondence to: D. Y. Wang  
(dwang@unb.ca)

systematic error of  $\sim 2\%$ . For the vertical profiles, the biases between the MIPAS and FTIR data are generally below 10% in the altitudes of 10 to 30 km. The MIPAS and SAFIRE  $\text{HNO}_3$  data generally match within their total error bars for the mid and high latitude flights, despite the larger atmospheric inhomogeneities that characterize the measurement scenario at higher latitudes. The MIPAS and ASUR comparison reveals generally good agreements better than 10–13% at 20–34 km. The MIPAS and IBEX measurements agree reasonably well (mean relative differences within  $\pm 15\%$ ) between 17 and 32 km. Statistical comparisons of the MIPAS profiles correlated with those of Odin/SMR, ILAS-II, and ACE-FTS generally show good consistency. The mean differences averaged over individual latitude bands or all bands are within the combined instrument errors, and generally within 1, 0.5, and 0.3 ppbv between 10 and 40 km ( $\sim 260$  and 4.5 hPa) for Odin/SMR, ILAS-II, and ACE-FTS, respectively. The standard deviations of the differences are between 1 to 2 ppbv. The standard deviations for the satellite comparisons and for almost all other comparisons are generally larger than the estimated measurement uncertainty. This is associated with the temporal and spatial coincidence error and the horizontal smoothing error which are not taken into account in our error budget. Both errors become large when the spatial variability of the target molecule is high.

## 1 Introduction

Space-based measurements are essential for monitoring the behaviour and trends of chemical species in the atmosphere since a global set of simultaneously derived atmospheric parameters can be obtained. Nitric acid ( $\text{HNO}_3$ ) is formed in the atmosphere either by gas phase reaction (Austin et al., 1986) and ion cluster reactions (Böhringer et al., 1983) or, less probable in the higher stratosphere, by heterogeneous reactions on sulphate aerosols (de Zafra et al., 2001). Early  $\text{HNO}_3$  observations from space were performed by the Atmospheric Trace Molecule Spectroscopy (ATMOS) experiment in a series of Space Shuttle-based missions during 1985 to 1994 (Gunson et al., 1996; Abrams et al., 1996).

The existence of  $\text{HNO}_3$  is found to be a key component in the photochemistry of stratospheric ozone destruction through its role in the formation of Type I Polar Stratospheric Clouds (PSCs) and as a main reservoir for the reactive nitrogen oxides (World Meteorological Organization, 2003). The global distribution of  $\text{HNO}_3$  concentration has been measured from satellite observations, such as the Limb Infrared Monitor of the Stratosphere (LIMS) instrument, mounted on the Nimbus-7 satellite (Gille and Russell, 1984), the Cryogenic Limb Array Etalon Spectrometer (CLAES) (Kumer et al., 1996) and the Microwave Limb Sounder (MLS) onboard the Upper Atmosphere Research Satellite (UARS) (Santee et al., 1999, 2004) and on Aura (Santee et al., 2005), the

Cryogenic Infrared Spectrometers and Telescopes for the Atmosphere (CRISTA) experiment aboard the Shuttle Pallet Satellite (SPAS) (Riese et al., 2000), the Improved Limb Atmospheric Spectrometer (ILAS) onboard the Advanced Earth Observing Satellite (ADEOS) (Koike et al., 2000 and Irie et al., 2002) and ILAS-II on ADEOS-II (Irie et al., 2006), and the Sub-Millimetre Radiometer (SMR) on Odin (Murtagh et al., 2002; Urban et al., 2005), as well as the high-resolution Fourier Transform Spectrometer (FTS) on SCISAT-1, also known as Atmospheric Chemistry Experiment (ACE) (Bernath et al., 2005).

Recent measurements of  $\text{HNO}_3$  volume mixing ratios (VMRs) in the troposphere and stratosphere are also provided by the Michelson Interferometer for Passive Atmospheric Sounding (MIPAS) (Fischer et al., 1996; European Space Agency, 2000) onboard the ENVISAT satellite. The instrument is a high resolution Fourier transform spectrometer and measures vertical profiles of temperature and various gas species by limb observations of mid-infrared emissions. The operational Level 1B and level 2 data have been produced by ESA using the operational retrieval algorithm (Raspollini et al., 2006; Carli et al., 2004).

The updated ESA version 4.61  $\text{HNO}_3$  data have been validated successfully against balloon-borne, aircraft and ground-based measurements (Oelhaf et al., 2004), though the reported validation cases have been confined to the re-analyzed operational MIPAS data almost only for the year 2002 and to mid-latitudes. The ESA MIPAS  $\text{HNO}_3$  profiles are also validated by comparison with the measurements from the far Infrared Balloon Experiment (IBEX) (Mencaraglia et al., 2006). Recently, Vigouroux et al. (2007) compared the ESA MIPAS  $\text{HNO}_3$  profiles with regular ground-based Fourier Transform InfraRed (FTIR) measurements for the year 2003 at 5 stations in both hemispheres, i.e. Jungfraujoch ( $46.5^\circ \text{N}$ ) and Kiruna ( $68^\circ \text{N}$ ), Wollongong ( $34^\circ \text{S}$ ), Lauder ( $45^\circ \text{S}$ ), and Arrival Heights ( $78^\circ \text{S}$ ). After making some corrections to take into account the known bias due to the use of different spectroscopic parameters, the comparisons of  $\text{HNO}_3$  partial columns show biases below 3% and standard deviations below 15% for all the stations except Arrival Heights (bias of 5%, standard deviation of 21%). The results at this latter station, where  $\text{HNO}_3$  has a larger spatial variability, highlight the necessity of defining appropriate collocation criteria and of accounting for the spread of the observed airmasses.

Complementary to the ESA operational data products, there are six different off-line data processors at five institutions for science-oriented data analysis of the high resolution limb viewing infrared spectra (von Clarmann et al., 2003a). The  $\text{HNO}_3$  VMR profiles produced by the MIPAS data processor developed at the Institut für Meteorologie und Klimaforschung (IMK) and complemented by the component of non-local thermodynamic equilibrium (non-LTE) treatment from the Instituto de Astrofísica de Andalucía (IAA) have been validated by Mengistu Tsidu et al. (2005), Stiller et al.

(2005), and Wang et al. (2007). The ESA operational  $\text{HNO}_3$  data are also compared with the IMK-IAA profiles taken on 42 days between September 2002 and December 2003 (Wang et al., 2007) and covering the whole latitude range of MIPAS. Both datasets generally show good consistency.

Increasing amount and enhanced diversity of MIPAS  $\text{HNO}_3$  products demand for even increased efforts in validation. A validation meeting was held on 29–30 November 2005 at Karlsruhe, Germany, to coordinate the activities. The validation data sets have been reprocessed after the meeting so the results are different from those reported in the previous documents (e.g. Vigouroux et al., 2007). This study focuses on the validation of the ESA operational  $\text{HNO}_3$  data version 4.61/4.62 and, in particular, on the comparisons with other coincident satellite observations for cross check. The profiles of the ESA-retrieved MIPAS operational  $\text{HNO}_3$  data are compared with 1) the ground-based FTIR measurements at five stations at mid and high latitudes of both hemispheres (Sect. 4); 2) the MIPAS STRatospheric (MIPAS-STR) (aircraft-based version of MIPAS) measurements and the Spectroscopy of the Atmosphere by using Far-InfraRed Emission – Airborne (SAFIRE-A) measurements (Sect. 5.1), as well as the Airborne Sub-millimetre Radiometer (ASUR) observations (Sect. 5.2); 3) field campaign data obtained from the balloon-borne version of MIPAS (MIPAS-B, Sect. 6.1), the infrared spectrometer MkIV (Sect. 6.2), the tunable diode laser instrument SPIRALE (Spectromètre Infra Rouge pour l'étude de l'Atmosphère par diodes Laser Embarquées, Sect. 6.3), and the Infrared Balloon Experiment (IBEX, Sect. 6.4); and 4) other satellite observations, such as from the SMR instrument on Odin (Sect. 7.1), from ILAS-II on ADEOS-II (Sect. 7.2), as well as from the FTS on ACE (Sect. 7.3). The characteristics of the ESA MIPAS data are outlined in Sect. 2, while our comparison method is described in Sect. 3. The reference data sets and their comparison results with the MIPAS data are presented in Sects. 4 to 7. Our conclusions are contained in Sect. 8.

## 2 The MIPAS operational data

Data to be validated here are the vertical profiles of abundances of  $\text{HNO}_3$  measured by MIPAS/ENVISAT during the period July 2002 to March 2004. The data sets are version 4.61/4.62 retrieved with the ESA operational data processor from the MIPAS spectra. The MIPAS observations provide global coverage with 14.4 orbits per day. The standard observation mode covers nominal tangent altitudes in a scanning sequence from the top 68 km down to 60, 52, and 47 km, and between 42 and 6 km at a step width of  $\sim 3$  km. The horizontal sampling interval is  $\sim 500$  km along-track and  $\sim 2800$  km across-track at the equator. The operational  $\text{HNO}_3$  profiles are retrieved based on the most recent re-processed L1B data version 4.61/4.62, with a vertical resolution of  $\sim 3$  km.

The tangent altitudes are registered by the engineering measurements. These are based on the satellite's orbit and attitude control system using star tracker information as a reference (called engineering data henceforth). The calibrated L1B spectra are analyzed using a global fit approach (Carlotti, 1988) by varying the input parameters of the forward model according to a non-linear Gauss-Newton procedure. In a first step, temperature and pressure at the engineering tangent altitudes are retrieved simultaneously (p, T retrieval), then the VMR profiles of the primary target species  $\text{O}_3$ ,  $\text{H}_2\text{O}$ ,  $\text{CH}_4$ ,  $\text{N}_2\text{O}$ ,  $\text{HNO}_3$  and  $\text{NO}_2$  are retrieved individually in sequence. Detailed descriptions of the operational retrieval algorithm have been reported by Ridolfi et al. (2000), Carli et al. (2004), and Raspollini et al. (2006).

Details about the retrieval error budget for the ESA operational  $\text{HNO}_3$  data have been reported by Dudhia et al. (2002). The MIPAS noise error is the covariance matrix given in the MIPAS level 2 operational products. We have taken the systematic errors from the Oxford web page (<http://www.atm.ox.ac.uk/group/mipas/err>). The error analysis for the nominal sets of microwindows used in both Near Real Time (NRT) and Off-Line (OFL) processing in normal MIPAS operations has been evaluated for 5 different atmospheric conditions, i.e. mid-latitude day-time (similar to the U.S. Standard Atmosphere), mid-latitude night-time, polar summer day-time, polar winter night-time, and equatorial day-time. A global composite of results for the five atmospheres, with twice the weight given to results from the polar winter case, is also provided. For  $\text{HNO}_3$  VMR profiles, the global random, systematic, and total errors are about 3.8%, 6.2%, and 7.3%, respectively, at 24 km altitude near the concentration peak, but increase to 35–50%, 20–25%, and 40–55% at 9 km and 42 km altitudes. In the present analysis, contrary to the approach of Oxford, we have considered the PT-error as a systematic error with random variability and added this to the noise error term. We decided to handle the error propagation from MIPAS-retrieved temperature profiles into  $\text{HNO}_3$  volume mixing ratios in this way since for statistical comparisons over a large number of profiles the temperature error is also mainly of a random nature. This procedure is in agreement with other MIPAS validation papers, e.g. Wetzel et al. (2007).

## 3 Comparison methods

For comparisons between individual profiles, the MIPAS and other data sets are searched for coincident measurements. The coincidence criteria of horizontal separation less than 300 km and time difference less than 3 h are used. This choice is based on our empirical knowledge of satellite data validation, and is to reduce the influence of small-scale gravity waves and large horizontal gradients at high latitudes. However, due to the characteristics of the data sampling scenarios, other more or less restricted coincidence criteria

have also been applied. Nevertheless, the numbers of available coincidence profiles vary from case to case from several hundreds to low tens, or even far less for most of the balloon measurements. This implies different statistical significance for the comparisons. Details will be discussed later in Sects. 4 to 7. Also, to avoid the influence of the error in the ESA MIPAS altitude registration (von Clarmann et al., 2003b; Wang et al., 2005; Kiefer et al., 2007), the comparisons are conducted in pressure coordinates.

When two correlative profiles with different vertical resolutions are compared, some small structures of the atmospheric field could be resolved by the higher resolution measurement, but not by the lower one. To account for this effect, the altitude (or pressure level) resolution should be adjusted using the averaging kernels. The method used is that described by Rodgers and Connor (2003), and its simplified application to our study is outlined below. Without loss of generality, the MIPAS data are assumed to have low resolution. The correlative high-resolution profiles are interpolated to a common grid, in this case to the pressure grid of the MIPAS data. The vertical resolution of the correlative profiles  $\mathbf{x}$  is adjusted by applying the averaging kernel of MIPAS  $\mathbf{A}_{\text{mipas}}$ . Also, the correlative profiles, which are assumed to be free of a priori information, are transformed to the a priori  $\mathbf{x}_{\text{mipas}}^a$  that is used by the MIPAS data. Both the a priori transformation and smoothing are done by

$$\tilde{\mathbf{x}} = \mathbf{A}_{\text{mipas}}\mathbf{x} + (\mathbf{I} - \mathbf{A}_{\text{mipas}})\mathbf{x}_{\text{mipas}}^a, \quad (1)$$

where  $\mathbf{I}$  is the unit matrix, and  $\tilde{\mathbf{x}}$  is the result derived with the MIPAS inverse model, if  $\mathbf{x}$  happens to be the true profile. More discussions about this transformation can be found in the paper of Wang et al. (2007).

The difference between the MIPAS measurement  $\mathbf{x}_{\text{mipas}}$  and the transformed other profile  $\tilde{\mathbf{x}}$  is

$$\begin{aligned} \delta &= \mathbf{x}_{\text{mipas}} - \tilde{\mathbf{x}} \\ &= (\mathbf{x}_{\text{mipas}} - \mathbf{x}) + (\mathbf{I} - \mathbf{A}_{\text{mipas}})(\mathbf{x} - \mathbf{x}_{\text{mipas}}^a), \end{aligned} \quad (2)$$

where the negative of the last term represents the differences originated from different vertical resolution and a priori. These contribute to the  $(\mathbf{x}_{\text{mipas}} - \mathbf{x})$  difference, but not to  $\delta$ . Thus, the residual  $\delta$  is taken as proxy for the discrepancy between the two measurements. For the  $i$ th pair of correlative profiles, the individual elements of the difference profile vector  $\delta_i$  at each pressure level  $z$  will be denoted as  $\delta_i(z)$  hereafter. The residuals  $\delta_i(z)$  are assembled in several ways (details are described in Sects. 4 to 7) for statistical analysis.

For each ensemble with  $N$  number of coincidence pairs, mean difference profiles  $\Delta(z)$  and their standard deviations  $\sigma(z)$  are calculated;  $\sigma(z)$  allows the precision of MIPAS profiles to be assessed. The statistical uncertainty in the mean difference  $\Delta(z)$  is quantified by  $\sigma(z)/N^{1/2}$ , which represents the uncertainty of  $\Delta(z)$  due to random-type errors. In the case of  $\Delta(z)$  being larger than  $\sigma(z)/N^{1/2}$ , their difference is an indicator of systematic errors between the comparison

data sets. We also compute the mean difference, standard deviation, and  $\sigma/N^{1/2}$  uncertainty averaged over pressure levels. These averaged quantities are directly evaluated according to the statistical definitions by assembling data points available at all pressure levels.

#### 4 Comparisons with ground-based FTIR measurements

The ESA MIPAS operational  $\text{HNO}_3$  data v4.61 recorded in the period of 26 July 2002 to 26 March 2004 were compared with the ground-based FTIR measurements at five stations at Jungfrauoch, Switzerland (46.5° N, 8.0° E), Wollongong, Australia (34.4° S, 150.5° E), Lauder, New Zealand (45.0° S, 169.7° E), Arrival Heights, Antarctica (77.5° S, 166.4° E), and Kiruna, Sweden (67.8° N, 20.4° E). All stations agreed in using the HITRAN2004 database in order to avoid biases due to different spectroscopic parameters. In the HITRAN2004 database (Rothman et al., 2005) and the MIPAS database (MIPAS pf3.1 for the v4.61/4.62 products; see Raspollini et al., 2006), the  $\text{HNO}_3$  line positions and intensities in the 11- $\mu\text{m}$  region that is used for the retrievals, are indeed following the same improvements based on laboratory measurements (Flaud et al., 2003). The present work is an update of a previous validation paper (Vigouroux et al., 2007) where the FTIR retrievals were made using the HITRAN2000 database. A high bias of about 14% was found between MIPAS and FTIR partial columns, which is in agreement with the differences in  $\text{HNO}_3$  line intensities in the HITRAN2000 and MIPAS pf3.1 databases.  $\text{HNO}_3$  profiles – with low vertical resolution – are retrieved from the absorption line shapes using a semi-empirical implementation of the Optimal Estimation Method (Rodgers, 1990, 2000). At Kiruna, the retrieval is performed with the inversion code PROFFIT (PROFile FIT) (Hase, 2000) and the forward model KOPRA (Karlsruhe Optimized Precise Radiative transfer Algorithm) (Höpfner et al., 1998) while the other stations use the retrieval algorithm SFIT2 (Pougatchev and Rinsland, 1995; Pougatchev et al., 1995; Rinsland et al., 1998). It has been shown in Hase et al. (2004) that both algorithms give similar results (within 1% for  $\text{HNO}_3$  total columns amount) under similar retrieval conditions.

The correlative measurements of FTIR and MIPAS were selected by coincidence criteria of time difference less than 3 h and horizontal distance less than 300 km at the MIPAS nominal tangent height of 21 km. Only at the Kiruna station have we applied an additional coincidence criterion of potential vorticity (PV) difference smaller than 15%. The MIPAS profiles have been degraded to the lower vertical resolution of the ground-based FTIR measurements using the FTIR averaging kernels (see Sect. 3, but in contrast to the case described there, MIPAS profiles have a higher resolution than those of FTIR). The MIPAS partial columns have been calculated from the smoothed profiles. We have evaluated the

combined random error covariance matrix of the difference (MIPAS – FTIR) (see Vigouroux et al., 2007, for more details). The FTIR random error budget has been estimated for a typical measurement at Kiruna. The error covariance matrix due to the noise is given in the MIPAS level 2 products for each profile. We have chosen to use, as the noise contribution to the MIPAS random error matrix, the mean of the covariance matrices of the coincident MIPAS profiles. Following the approach adopted for the MIPAS comparison with other satellite measurements, we have added the systematic errors with random variability to the MIPAS random error budget (i.e. PT-error; see Sect. 2).

Figure 1 shows the time series of partial columns at the ground-based stations, except for Wollongong where only one coincidence occurs. For both instruments seasonal variations are captured well at the four ground-based stations Jungfraujoch, Lauder, Arrival Heights, and Kiruna. The pressure ranges defining the partial columns and the numbers of coincidences for these comparisons are given in Table 1. The low pressure limits are chosen based on the ground-based FTIR sensitivity which varies from station to station, and which is good up to  $\sim 28$ , 32, 36, and 43 km (18, 9, 5, and 2 hPa, resp.), for Jungfraujoch, Lauder, Arrival Heights, and Kiruna, respectively. The high pressure limits of partial columns are determined by the lowest altitudes of the MIPAS profiles, which have a mean value of about 12 km. MIPAS profiles for which the lowest altitude is higher than 12 km have not been used for the calculation of partial columns. Table 1 also gives the means (M), standard deviations (STD), and the combined random errors and standard errors on the means (SEM) of the relative partial column differences at the five stations. For calculation of mean relative differences, the mean absolute difference of (MIPAS – FTIR) has been divided by the mean FTIR partial column. The SEM are calculated as  $3 \times \text{STD} / \sqrt{N}$  with  $N$  being the number of coincidences, in order to distinguish with 99% of confidence whether the biases are statistically significant.

As shown in Table 1, the mean relative differences between the MIPAS and FTIR  $\text{HNO}_3$  partial columns are within  $\pm 2\%$ , and the statistical standard errors on the means are 6–11% for the Jungfraujoch, Arrival Heights, Lauder, and Kiruna stations. The MIPAS systematic error for the partial columns is around 2%. Considering these factors, we can conclude that there is no statistically significant bias between the MIPAS and FTIR partial columns in the considered pressure ranges, for the Jungfraujoch, Lauder, Arrival Heights, and Kiruna stations. The statistical standard deviations of Jungfraujoch, Arrival Heights, Lauder, and Kiruna stations (where the number of coincidences is reasonable for statistical conclusions) are 13%, 11%, 5%, and 9%, respectively. These values are larger than the estimated random error of about 3% on the relative difference of the partial columns. These large standard deviations, compared to the estimated random error, should be explained by the temporal and spatial coincidence errors and the horizontal smoothing

error which are not taken into account in our error budget. Both errors become large when the spatial variability of the target molecule is high (see von Clarmann, 2006; Cortesi et al., 2007). No conclusions can be drawn for the Wollongong station because there is only one coincidence. Nevertheless, considering the SEM obtained for the other stations, the observed bias at Wollongong of  $-5.7\%$  may be assumed to be non-significant.

Figure 2 displays the means and the  $1\text{-}\sigma$  standard deviations of the relative differences between the ground-based FTIR and the MIPAS profiles at the five ground-based stations. The given combined random error (shaded area) is a combination of the random error of FTIR with the noise error and the systematic error with random variability of MIPAS. The  $3\text{-}\sigma$  standard error on the mean is also indicated to facilitate the discussion of the statistical significance of the observed bias. The profile comparisons confirm what has been seen for the partial columns comparisons. The bias is statistically insignificant and below 10% at Kiruna and Jungfraujoch in the whole altitude range and at Arrival Heights for altitudes lower than 15 hPa.

The result of Kiruna shows much smaller bias than those of Jungfraujoch, Wollongong, Lauder and Arrival Heights. The reason is not fully clear at the moment. The mean difference profiles show strong oscillations at Wollongong and Lauder. One should remember that the detailed shape of the FTIR profiles depends on the choice of retrieval parameters. In the present exercise Lauder and Wollongong used similar retrieval parameters. This could explain why we observe similar oscillations in the profile differences at these stations. Regarding the standard deviations, we can see in Fig. 2, that they are always larger than the combined random error, probably for the same reason than for partial column comparisons: the coincidence errors of the sounded airmasses and the horizontal smoothing errors are not taken into account in the error budget.

## 5 Comparisons with aircraft-borne instruments

### 5.1 SAFIRE-A and MIPAS-STR

SAFIRE-A (Spectroscopy of the Atmosphere by using Far-InfraRed Emission – Airborne) is a high-resolution FT instrument, performing limb emission measurements in narrow bands ( $\sim 1\text{--}2\text{ cm}^{-1}$ ) within the far-infrared spectral region ( $10\text{--}250\text{ cm}^{-1}$ ), as described by Bianchini et al. (2004). MIPAS-STR (MIPAS STRatospheric aircraft) is an aircraft version of the MIPAS satellite spectrometer and operates in the middle infrared spectral region with similar characteristics and performances (Piesch et al., 1996). Both instruments obtain  $\text{HNO}_3$  profiles from the upper troposphere up to the flight altitude and the total  $\text{HNO}_3$  column above. SAFIRE-A mean profiles have been calculated over fixed pressure levels, corresponding approximately to a regular altitude grid with

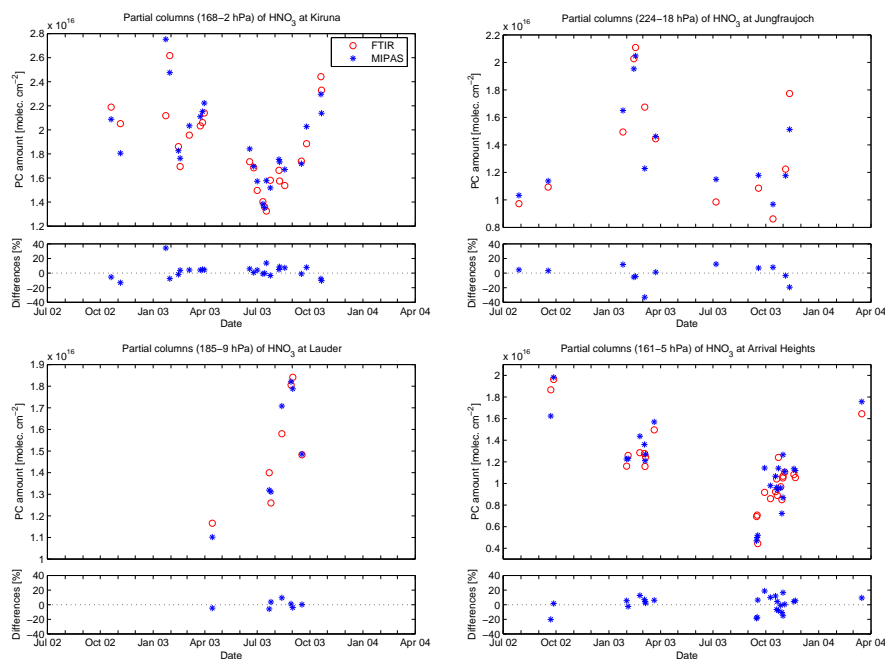


**Fig. 1.** Time series of ground-based FTIR (red circles) and ESA operational MIPAS (blue stars)  $\text{HNO}_3$  partial columns (large panels) and their relative differences (small panels) at four stations: Kiruna (top-left), Jungfraujoch (top-right), Lauder (bottom-left), and Arrival Heights (bottom-right). The pressure ranges used for the partial columns are given in the titles. The relative differences are calculated as  $(\text{MIPAS}-\text{FTIR})/\text{mean}(\text{FTIR})$ .

**Table 1.** Statistical means (M) and standard deviations (STD) of the relative differences  $(\text{FTIR}-\text{MIPAS})/\text{mean}(\text{FTIR})$  (in percent) of the  $\text{HNO}_3$  partial columns in the given pressure ranges. The numbers of coincidences between the MIPAS and collocated ground-based FTIR measurements within 3 h and 300 km for the statistical comparisons are given in parentheses behind each station name. The combined random errors on the differences and  $3\text{-}\sigma$  standard errors on the means (SEM) are also listed.

Station	Pressure Range (hPa)	M $\pm$ STD %	Random Error %	Standard Error on M (SEM) ( $3\sigma$ ) %
Jungfraujoch (12)	18–224	$-1.5 \pm 13.2$	2.8	11.4
Wollongong (1)	12–196	$-5.7$	2.9	–
Lauder (7)	9–185	$+0.0 \pm 5.4$	2.7	6.1
Arrival Heights (26)	5–161	$+1 \pm 10.7$	2.4	6.3
Kiruna (24)	2–168	$+2.3 \pm 9.4$	3.0	5.8

steps of 1.0 km. MIPAS-STR profiles have been retrieved on a fixed altitude grid (Höpfner et al., 2001 and Keim et al., 2004). Their vertical resolution (approximately 1–2 km) is slightly better, but still comparable with the one of MIPAS ESA operational v4.61/v4.62 data. Therefore, the data are directly compared with the satellite measurements without correcting for the vertical smoothing effects.

The error budget estimates are reported for both instruments. For a single profile, the random errors for MIPAS-

STR and SAFIRE-A are between 4 and 2% ( $1\sigma$ ). The systematic error in MIPAS-STR profiles is about 6%, mainly due to temperature used to obtain the trace gases. No HI-TRAN error is considered for MIPAS-STR since the same spectral bands are used as in case of MIPAS/ENVISAT. The estimate of the systematic error in the SAFIRE-A profiles takes into account the contribution of the assumed (not retrieved from the measurements) pressure and temperature profile ( $\sim 2\%$ ) and the spectroscopic error ( $\sim 5\%$  as an upper

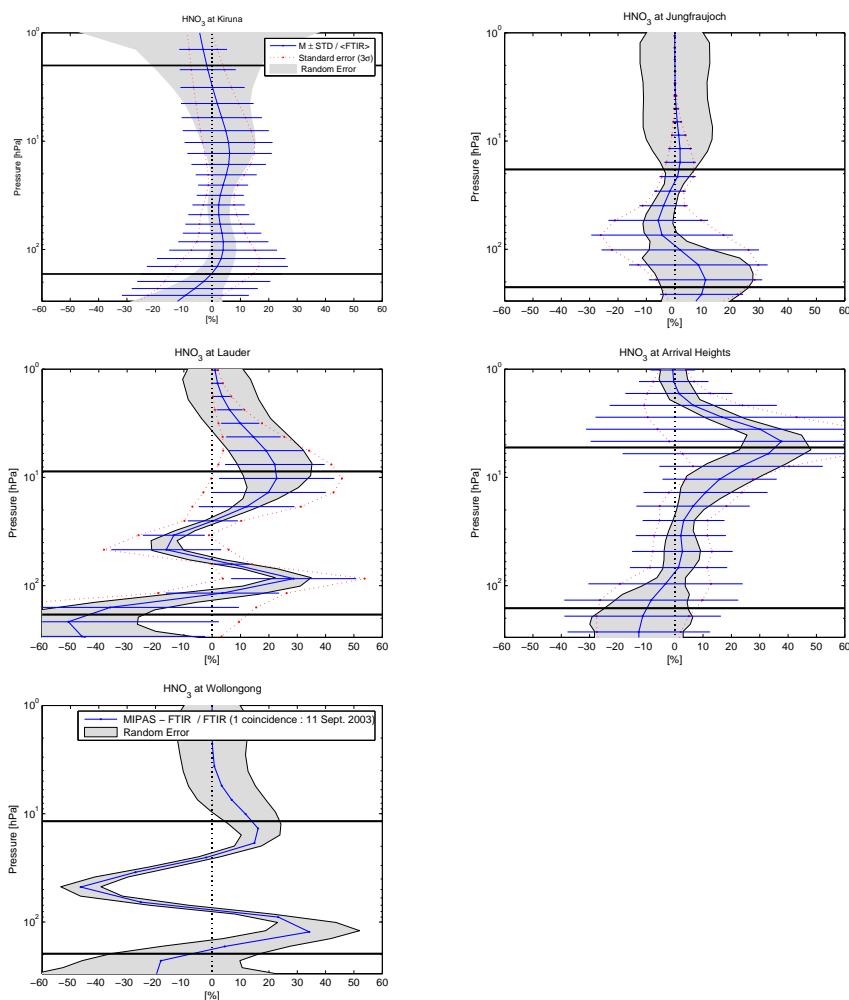


**Fig. 2.** Statistical means (blue line) and standard deviations (error bars) of the relative differences (FTIR-MIPAS)/FTIR (in percent) of the HNO<sub>3</sub> profiles, where MIPAS are the ESA operational data and FTIR measurements are taken at 5 stations: Kiruna (top-left), Jungfraujoch (top-right), Lauder (middle-left), Arrival Heights (middle-right), Wollongong (bottom). The red dots indicate the 3- $\sigma$  standard error on the mean, and the shaded areas correspond to the estimated random error on the relative differences. The two black horizontal bars show the pressure ranges used for the partial columns listed in Table 1.

limit and a better estimate around 2%). Effects such as non-LTE, uncertainties in the pointing of the instrument, horizontal atmospheric inhomogeneity along the line of sight can cause further errors, which were considered of minor importance.

The two FT spectrometers flew aboard the M-55 Geophysical stratospheric high altitude aircraft. A total of 11 flights and about 45 flight hours was performed for the validation of the ENVISAT chemistry payload in the frame of the 2002–2003 ESABC (ENVISAT Stratospheric Aircraft and Balloon Campaign) field campaigns at mid-latitude (Forlì, Italy, July and October 2002) and in the Arctic region (Kiruna, Sweden, February–March 2003), as reported in details by Cortesi

et al. (2004). Figures 3 and 4 show the SAFIRE observation configurations for two flights on 24 October 2002 and 2 March 2003, respectively. The aircraft measurements conducted in the polar region (Fig. 4) aimed at validating MIPAS/ENVISAT products in presence of strong vertical and horizontal gradients; consequently, the corresponding datasets (February–March 2003 data) generally includes data acquired at the border of the polar vortex, with vertical and horizontal inhomogeneities much larger than those encountered at mid-latitude (July and October 2002 data). To avoid strong gradients along the line of sight of the remote sensing instruments, which decrease the quality of the measured profiles, the flights were planned with long north-south legs.

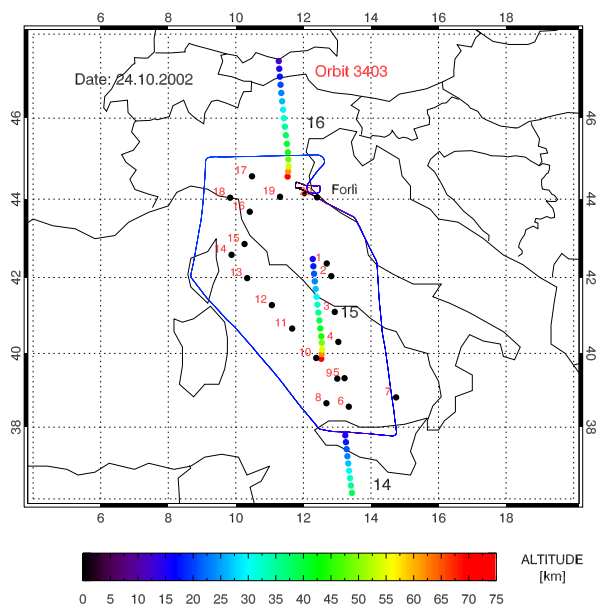


**Fig. 3.** Map of M-55 Geophysica route (blue) during the ENVISAT validation flights at Forlì, Italy (42° N, 12° E) on 24 October 2002. The geolocations and tangent altitudes of MIPAS/ENVISAT tangent points for the selected overpasses (numbered as scans 14–16 of orbit 3403) are indicated by the color codes. The geographical coverage (black circles) and the scan sequence numbers (red) of collocated aircraft measurements by SAFIRE, in coincidence with MIPAS/ENVISAT are also denoted. For the coincident measurements, their differences in time, latitude and longitude, and horizontal distance see Table 2.

The aircraft measurements have been performed in west-east direction, while the MIPAS/ENVISAT measured north-south along the gradients.

Using these data, multiple coincidences can be identified – based on the matching criteria ( $\Delta s < 300$  km,  $\Delta t < 3$  h) – between MIPAS/ENVISAT and the remote sensing and in situ aircraft observations, thus obtaining a comprehensive set of collocated  $\text{HNO}_3$  profiles to be considered for validation purposes. We have selected a subset of the above comparison pairs by choosing, for each MIPAS/ENVISAT scan, the  $\text{HNO}_3$  profiles measured with the best spatial and temporal coincidence by SAFIRE-A and MIPAS-STR. The resulting validation data sets have very high quality coincidences, both in the spatial and in the temporal domain, as listed in Tables 2 and 3 for SAFIRE and in Table 4 for MIPAS-STR during three high latitude campaigns at Kiruna, Sweden on 28 February, 2 March, and 12 March of year 2003.

Results of the comparison between MIPAS/ENVISAT  $\text{HNO}_3$  profiles and the SAFIRE-A correlative measurements obtained during northern mid-latitude flights (Forlì, Italy, 24 October 2002) and during the Arctic campaign (Kiruna, Sweden, 2 March 2003) are shown in Figs. 5 and 6, respectively.

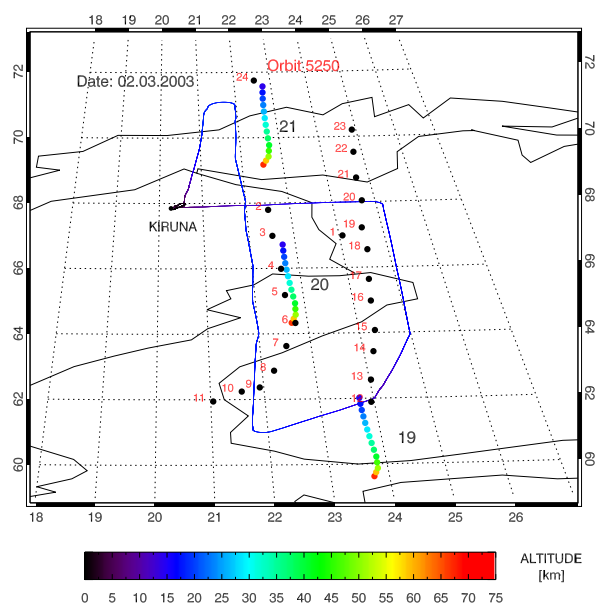


**Fig. 4.** Same as Fig. 3, but for the SAFIRE measurements on the M-55 Geophysica flight at Kiruna, Sweden (68° N, 20° E) on 2 March 2003. The MIPAS/ENVISAT observations are numbered as scans 19–21 of orbit 5250. For the coincident measurements, their differences in time, latitude and longitude, and horizontal distance see Table 3.

Each plot displays the  $\text{HNO}_3$  vertical distribution retrieved by MIPAS/ENVISAT for one of the selected overpasses, which is compared with the mean VMR profile of SAFIRE-A obtained by averaging over all the limb scanning sequences collocated with the selected satellite overpass. The comparisons cover the altitude range between  $\sim 25$  km (slightly above the maximum flight altitude) and MIPAS/ENVISAT lowest tangent altitude. The error bars on MIPAS/ENVISAT, and SAFIRE-A profiles indicate the total uncertainty on the corresponding  $\text{HNO}_3$  values.

Very good agreement is found at mid-latitude (Fig. 5). The SAFIRE  $\text{HNO}_3$  measurements and satellite data are generally matched within their total error bars. The only exception is the profile of MIPAS/ENVISAT orbit 3402/scan 16, that compared with a single profile of SAFIRE. Reasonably good results are found, on the other hand, also from the comparison of the SAFIRE  $\text{HNO}_3$  profiles from the Arctic flight Fig. 6, despite the larger atmospheric inhomogeneities that characterize the measurement scenario at higher latitudes. The occurrence of strong vertical gradients is highlighted in the comparison with SAFIRE measurements (see, for instance, the profile of MIPAS/ENVISAT orbit 5250/scan 21) and can account for the observed differences with the satellite data, whilst horizontal gradients encountered at the border of the polar vortex might at least partially justify the discrepancy in  $\text{HNO}_3$  values retrieved by the airborne and satellite limb-sounders.

**Table 2.** Coincident measurements between SAFIRE and MIPAS scans of orbit 3403 on 24 October 2002. See Fig. 3 for the absolute geolocations.

MIPAS scan	SAFIRE scan	$\Delta t$ [min]	$\Delta \text{lat}$ [degree]	$\Delta \text{lon}$ [degree]	$\Delta s$ [km]
14	5	102	-1.85	0.05	205.9
14	6	95	-1.07	-0.07	119.8
14	7	86	-1.33	-1.47	196.3
14	8	62	-1.17	0.59	140
14	9	53	-1.84	0.27	205.7
14	10	46	-2.39	0.89	277.4
15	1	135	-0.17	-0.39	37.8
15	2	128	0.16	-0.52	46.3
15	3	119	1.09	-0.62	132.1
15	4	112	1.89	-0.73	218.6
15	10	47	2.31	-0.07	257.7
15	11	38	1.53	0.64	178.6
15	12	30	0.91	1.24	144.6
15	13	21	0.21	1.97	164.4
15	14	14	-0.39	2.43	204.8
15	15	5	-0.67	2.05	184
15	16	-1	-1.49	1.89	226.7
15	18	-18	-1.84	2.47	287.4
15	19	-27	-1.87	1.00	223.1
15	20	-34	-1.85	-0.10	206.6
16	17	-9	2.42	0.83	277.1

Comparisons between MIPAS/ENVISAT and MIPAS-STR also show very good agreement at the northern mid latitude campaigns, as shown in Fig. 7 for three MIPAS measurements. The reason for the profile measured at 09:19 UTC (blue line) being too high might be a strong N-S gradient of  $\text{HNO}_3$  VMRs as indicated by the MIPAS/ENVISAT observations. Results of the comparisons between MIPAS/ENVISAT  $\text{HNO}_3$  profiles and the MIPAS-STR correlative measurements obtained during the three Arctic campaigns at Kiruna on 28 February, 2 March and 12 March in 2003 are shown in Figs. 8 to 10, respectively. Also shown in these figures are flight routes and observation configurations (top panels) of each campaign. The  $\text{HNO}_3$  vertical distribution retrieved by MIPAS/ENVISAT for one of the selected overpasses has been compared with the single VMR profile of MIPAS-STR collocated with the selected satellite overpass. We can notice from Figs. 8 to 10 that MIPAS/ENVISAT normally tends to be in a very good agreement with MIPAS-STR and only occasionally to show somewhat large differences, mostly in terms of a slight overestimate of the  $\text{HNO}_3$  VMR. The latter tendency is more pronounced in comparison with SAFIRE-A mean profiles, that are almost constantly lower than MIPAS/ENVISAT  $\text{HNO}_3$  values.

The observed differences could be explained by the fact that the selected collocated  $\text{HNO}_3$  profiles, satisfying the spatial and temporal coincidence criteria, can sample differ-

ent air masses across a region of strong horizontal (and vertical) gradients. From in-situ observations onboard the NASA ER-2 (Kawa et al., 1990), one can derive maximum values of the horizontal gradient for the Arctic of  $\text{NO}_y$  (which is mainly in the form of  $\text{HNO}_3$  at these latitudes) of up to 0.02 ppbv/km, which makes around 8 ppbv variation along the line-of-sight within a 3 km thick tangent layer of MIPAS. In NASA DC-8 in-situ observations of the lowest stratosphere in the Arctic winter 1988/89 even gradients of up to 0.13 ppbv/km are observed over short distances (Hübner et al., 1990). Over longer paths (200 km) a mean gradient of  $\text{NO}_y$  of about 0.05 ppbv/km is visible. As displayed in Fig. 9 for the potential vorticity field on the isentropic surface  $\Theta = 400$  K (approximately 16 km) in the region covered by the M-55 flight on 2 March 2003, the geolocation of the collocated measurements from MIPAS/ENVISAT (UT=20:37) and MIPAS-STR (UT=22:08) mostly overlaps on a region with PV values of about  $(15 \pm 1)$  pvu. In contrast, as seen in Fig. 4, the same MIPAS/ENVISAT scan (orbit 5250 – scan 21) was compared with the mean SAFIRE profile averaged over scans 21–24, which cover a more extended area including air masses with PV values as low as  $\sim 11$  pvu. Correspondingly, we observe matching  $\text{HNO}_3$  values retrieved at 16 km by MIPAS/ENVISAT and MIPAS-STR with differences less than 0.5 ppbv (Fig. 9), but significantly lower (by 3 ppbv)  $\text{HNO}_3$  VMR measured by SAFIRE-A (Fig. 6). Similar checks have been performed using

**Table 3.** Coincident measurements between SAFIRE and MIPAS scans of orbit 5250 on 2 March 2003. See Fig. 4 for the absolute geolocations.

MIPAS scan	SAFIRE scan	$\Delta t$ [min]	$\Delta \text{lat}$ [degree]	$\Delta \text{lon}$ [degree]	$\Delta s$ [km]
19	6	51	-2.59	0.99	292.6
19	7	43	-1.89	1.23	219.4
19	8	34	-1.14	1.52	149.2
19	9	27	-0.63	1.82	118.1
19	10	18	-0.51	2.16	126.4
19	11	11	-0.21	2.7	143.7
19	12	2	-0.15	-0.2	20.1
19	13	-4	-0.83	-0.28	93.6
19	14	-13	-1.7	-0.45	190.1
19	15	-21	-2.34	-0.57	262.1
20	1	93	-0.7	-1.33	97.8
20	2	84	-1.35	0.22	150.4
20	3	77	-0.55	0.2	62.2
20	4	68	0.46	0.1	51.2
20	5	61	1.26	0.09	140.5
20	6	52	2.12	-0.04	235.8
20	7	44	2.82	0.2	314
20	15	-20	2.37	-1.59	273.9
20	16	-29	1.47	-1.65	179.9
20	17	-36	0.8	-1.71	118.5
20	18	-45	-0.1	-1.83	82.1
20	19	-52	-0.77	-1.83	117.4
20	20	-61	-1.6	-1.98	197.2
20	21	-69	-2.3	-1.98	269.2
21	21	-67	2.54	-1.95	292.9
21	22	-76	1.76	-2.05	210.1
21	23	-83	1.08	-2.15	144
21	24	-92	-0.46	0.19	52.1

**Table 4.** Best temporal and spatial coincidences selected for MIPAS/ENVISAT HNO<sub>3</sub> validation with the MIPAS-STR measurements from M-55 Geophysica aircraft flights at Kiruna, Sweden (67.8° N, 20.4° E) in year of 2003. Each selected coincidence pair is specified by their UTC time. The corresponding latitude and longitude (in degrees) are given for altitude of 16 km. Also reported are their differences in time ( $\Delta t$  in hours), horizontal distance ( $\Delta s$  in kilometers), and potential vorticity ( $\Delta PV$  in  $10^{-6} \text{ K m}^2 \text{ kg}^{-1} \text{ s}^{-1}$ ) at 400 K potential temperature.

MIPAS-STR Date/UTC	lat/lon	MIPAS Date/UTC	lat/lon	$\Delta t$	$\Delta s$	$\Delta PV$
28 Feb/07:56	69.7/22.8	28 Feb/08:26	69.6/28.3	0.5	212	1
28 Feb/08:59	75.3/28.7	28 Feb/08:25	74.9/30.9	-0.6	79	0
2 March/19:20	66.6/23.7	2 March/20:35	66.6/22.7	1.2	42	0
2 March/20:30	61.8/24.7	2 March/20:34	61.9/23.7	0.1	52	0
2 March/22:08	70.9/26.8	2 March/20:37	71.5/22.8	-1.5	157	-1
12 March/07:59	69.6/18.6	12 March/08:49	69.6/22.5	0.8	151	-1
12 March/08:55	75.2/21.2	12 March/08:48	74.9/25.1	-0.1	114	0
12 March/09:17	78.3/17.7	12 March/08:46	79.6/22.8	-0.5	179	0
12 March/09:56	75.1/4.3	12 March/10:28	74.9/-0.0	0.5	126	-2

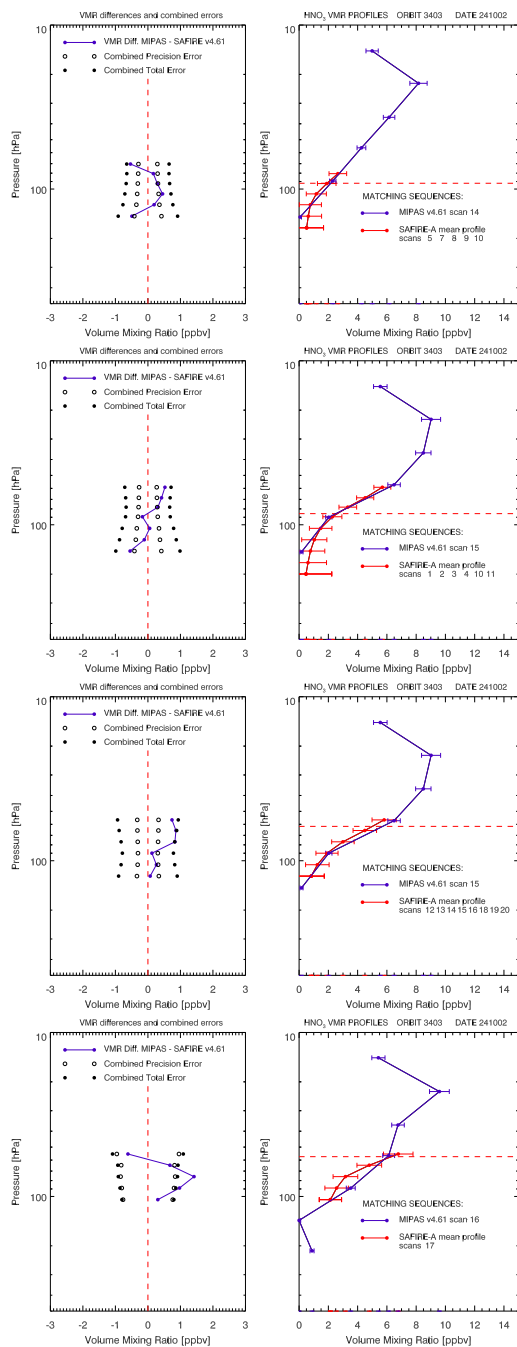


**Fig. 5.** Comparisons of  $\text{HNO}_3$  VMR (in ppbv) profiles (right panels) between MIPAS ESA operational data and correlative aircraft-based SAFIRE measurements (red) during the mid-latitude flight on 24 October 2002 from Forlì, Italy ( $42^\circ$  N,  $12^\circ$  E). The horizontal red dashed lines indicate the flight altitude of the airplane. The left panels show the differences (in ppbv of MIPAS minus SAFIRE) (blue), and the combined random (white circles) and systematic (black circles) errors.

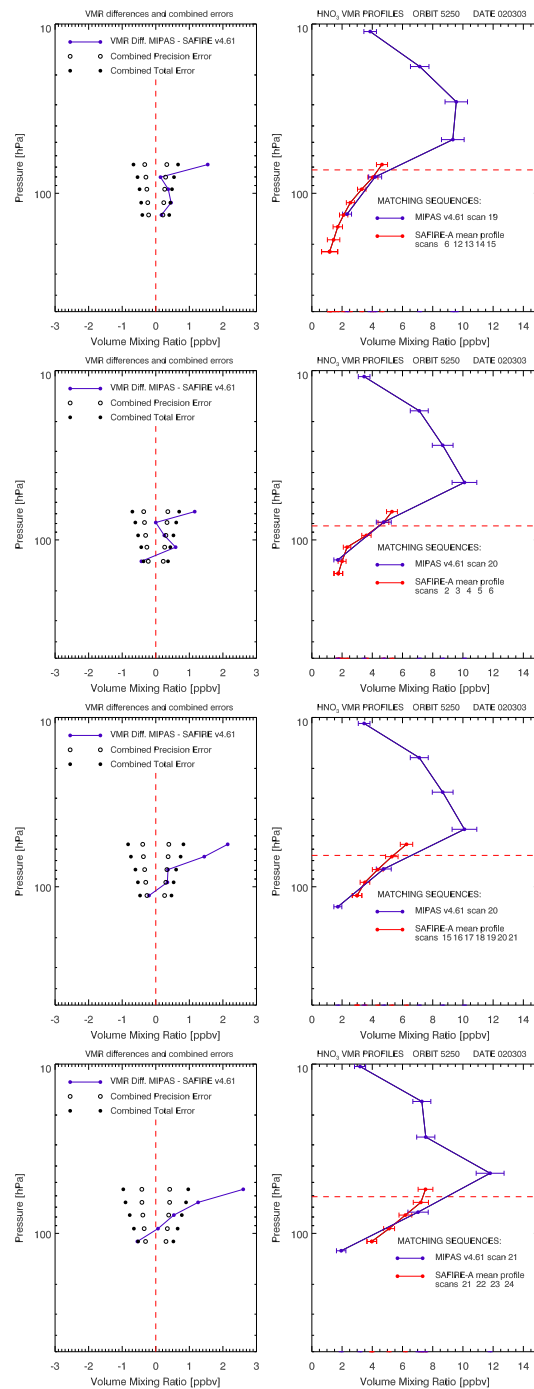


**Fig. 6.** Same as Fig. 5, but for the high latitude flight on 2 March 2003 from Kiruna, Sweden ( $68^\circ$  N,  $20^\circ$  E).

different combinations of coincident data, and confirmed that a significant difference between simultaneous  $\text{HNO}_3$  measurements of MIPAS/ENVISAT and one of the M-55 Geophysica sensors is mostly due to sampling of different air

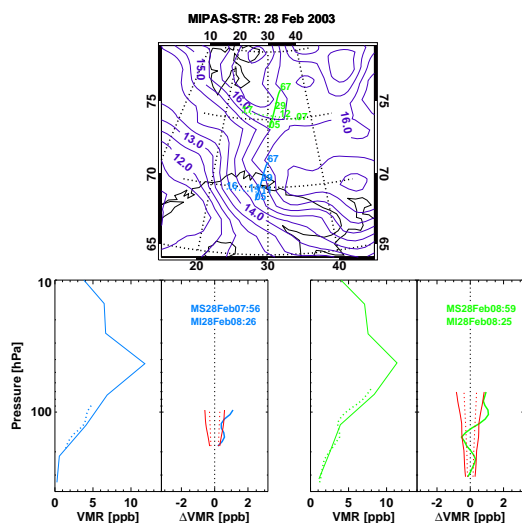


**Fig. 7.** Comparison of  $\text{HNO}_3$  volume mixing ratio (in ppbv) profiles observed by MIPAS/ENVISAT (solid) and aircraft-based MIPAS-STR measurements (dotted) at mid-latitudes (Forlì, Italy) on 22 July 2002. The top panel shows the flight and satellite tangent point tracks for the MIPAS-STR and MIPAS/ENVISAT measured sequences. The numbers indicate the altitudes (in kilometers) of selected flight and satellite tangent points. The bottom panels show the profiles (left) and their differences (right). In the difference panels, the combined noise error is red dotted and the combined total error (without errors from HITRAN) is red solid.

masses across a region of strong horizontal (and vertical) gradients.

## 5.2 ASUR

The Airborne Submillimeter Radiometer (ASUR) is a passive heterodyne sensor that operates in a tunable frequency range of 604.3–662.3 GHz (Mees et al., 1995; von König et al., 2000). The receiver carries two spectrometers, an Acousto Optical Spectrometer (AOS) and a Chirp Transform Spectrometer (CTS). Stratospheric measurements with the AOS are analyzed for this comparison study. The total bandwidth of the AOS is 1.5 GHz and its resolution is 1.27 MHz. The observations are performed onboard a research aircraft to avoid signal absorption due to tropospheric water vapor. The instrument looks upward at a constant zenith angle of  $78^\circ$ . Thermal emissions from the rotational states of the molecule (a rotational line band at 606.8 GHz for  $\text{HNO}_3$ ) are detected by the sensor and the shape of the pressure broadened lines can be related to its vertical distribution. The measured single spectra are integrated over 90 s to obtain a sufficient signal-noise-ratio. The horizontal resolution of the profile is  $\sim 20$  km, which depends on the aircraft speed and the integration time. The vertical profiles are retrieved on a 2 km grid applying the optimal estimation method (Rodgers, 1976). Altitude resolution of the  $\text{HNO}_3$  measurement is 6–

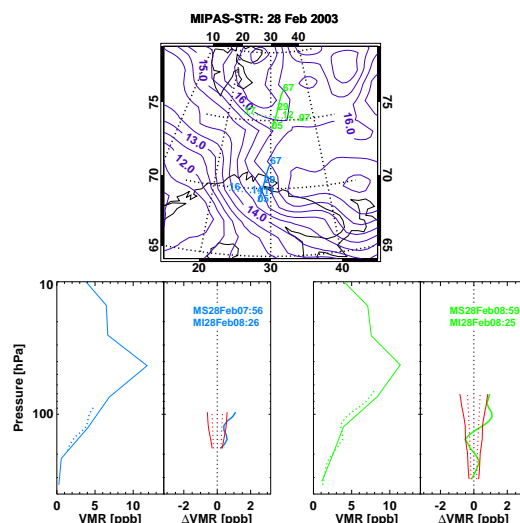


**Fig. 8.** Comparison of  $\text{HNO}_3$  volume mixing ratio (in ppbv) profiles observed by MIPAS/ENVISAT (solid) and aircraft-based MIPAS-STR measurements (dotted) at Kiruna, Sweden ( $68^\circ\text{N}$ ,  $20^\circ\text{E}$ ) on 28 February 2003. The top panel shows the flight and satellite tangent point tracks for the MIPAS-STR and MIPAS/ENVISAT measured sequences. The numbers indicate the altitudes (in kilometers) of selected flight and satellite tangent points. Overlaid violet contour lines are potential vorticity (in  $10^{-6} \text{K m}^2 \text{kg}^{-1} \text{s}^{-1}$ ) at 400 K potential temperature. The bottom panels show the profiles (the first and third column from the left) and their differences (the second and fourth column). In the difference panels, the combined noise error is the red dotted line and the combined total error (without errors from HITRAN) is the red solid line.

10 km in the lower stratosphere and the vertical range is 14–35 km (16–32 km for the tropical measurements). The precision of a typical measurement is 0.3 ppb and the estimated accuracy is about 0.6 ppb or 15%, whichever is higher (Kleinböhl et al., 2003, and von König et al., 2002). Further details about the ASUR  $\text{HNO}_3$  retrieval is given in Kuttippurath (2005).

The ASUR  $\text{HNO}_3$  measurements during the SCIAVALUE (SCIAMACHY Validation and Utilization Experiment) (Fix et al., 2005) and EuPLEx (European Polar Leewave Experiment) (Kleinböhl et al., 2005) campaign are taken for the comparison with MIPAS v4.61 data. The predefined criterion that the airborne measurements must be within 300 km and 3 h of the satellite observations is considered for the validation analysis. However, since the number of collocated measurements were too small (23 coincidences spread over a large latitudinal area), statistics were enhanced significantly by choosing also another more relaxed criterion,  $\sim 1000$  km and within  $\pm 12$  h, for the intercomparisons. This criterion resulted in a total of 768 collocated measurements from 21 ASUR measurement flights in September 2002, and in January, February, and March 2003. The date and flight track of these collocated measurements are given in Table 5.

**Table 5.** The date and flight track of the ASUR collocated measurements. More relaxed criterion,  $\sim 1000$  km and within  $\pm 12$  h, is chosen for the intercomparisons. The number of collocated measurements for the criterion  $\pm 300$  km in 3 h is shown in parenthesis.

Date	Flight Track	Number of Coincidences
Sep 2002		
17 Sep 2002	Palma de Mallorca-Niamey	04 (06)
18 Sep 2002	Niamey-Nairobi	03
25 Sep 2002	Nairobi-Niamey-Djerba	05
26 Sep 2002	Djerba-Palma de Mallorca	35 (08)
Jan 2003		
14 Jan 2003	Munich-Kiruna	44
19 Jan 2003	In the Arctic	93
23 Jan 2003	In the Arctic	90
26 Jan 2003	In the Arctic	04
Feb 2003		
7 Feb 2003	In the Arctic	138
8 Feb 2003	In the Arctic	138
9 Feb 2003	In the Arctic	19
19 Feb 2003	Munich-Basel-Tozeur	02
24 Feb 2003	Nairobi-Mombasa-Seychelles	01
26 Feb 2003	Seychelles-Nairobi	02
28 Feb 2003	Nairobi-Douala	07
March 2003		
10 March 2003	Munich-Kiruna	47 (01)
12 March 2003	Kiruna-NyAalesund-Kiruna	97 (07)
13 March 2003	Kiruna-Keflavik	26 (01)
14 March 2003	Keflavik-Kangerlussuaq <sup>a</sup>	03
15 March 2003	Kangerlussuaq-Keflavik	02
19 March 2003	Munich Local flight	08
Total		768 (23)

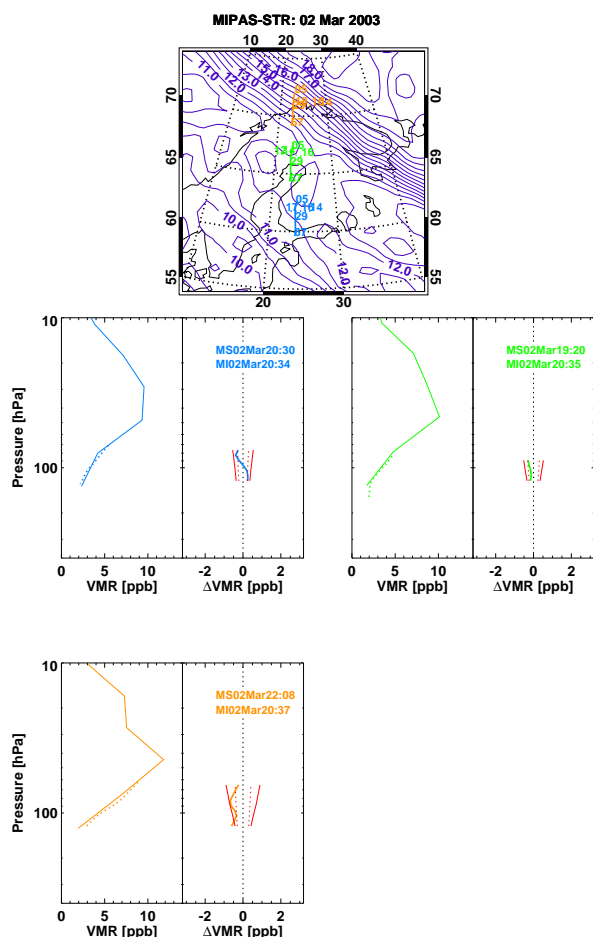
The MIPAS  $\text{HNO}_3$  VMRs are convolved with the ASUR  $\text{HNO}_3$  averaging kernels to account for lower vertical resolution of the ASUR profiles. The differences ( $\Delta\text{VMR} = \text{MIPAS VMR} - \text{ASUR VMR}$ ) are calculated from the individual MIPAS and ASUR profile comparisons (an example is shown in Fig. 11). The resulting delta profiles are averaged over the low latitudes (5 S–30 N), mid-latitudes (30 N–60 N), and high latitudes (60 N–90 N). The analysis results are presented in terms of these latitude sections separately.

Figure 12 (blue curves) shows the results from the comparison between ASUR and MIPAS profiles with the pre-defined criterion, 300 km and 3 h. There are 6 coincident measurements in the tropics, 9 in mid-latitudes and 8 in high-latitudes. Between 20 and 34 km, the differences range from  $-0.4$  to  $+0.7$  ppb or  $-25$  to  $+30\%$  in the tropics, up to  $0.7$  ppb or  $15\%$  in the mid-latitudes and  $-0.3$  to  $+0.1$  ppb or  $-5$  to  $+2\%$  in the high latitudes. The average MIPAS–ASUR deviation is  $-0.1$  to  $+0.4$  ppb or  $-5$  to  $+13\%$  above 20 km. The differences are highest in the tropics and lowest in the high-latitudes.

Figure 12 (red curves) also shows the results from the comparison between ASUR and MIPAS profiles with the additional criterion of 1000 km and 12 h. There are 36

**Table 6.** Numbers of correlative profiles used for  $\text{HNO}_3$  comparison: data from balloon-borne MIPAS-B and MkIV measurements, as well as other satellite observations. See the text for coincidence criteria. One MIPAS profile may have multiple coincidences. This is indicated by paired numbers with the first for MIPAS and the second for the correlative measurements.

Data Set	Time Period	Coincidences
MIPAS-B	24 Sep 2002	1/1
		2/1
MIPAS-B	20/21 March 2003	3/1
		3/1
MIPAS-B	3 July 2003	3/1
		3/1
MkIV	16 Dec 2002	3/1
MkIV	1 April 2003	4/1
MkIV	20 Sep 2003	6/1
Odin/SMR	19 Sep 02–28 Feb 2003	706/960
ILAS-II	12 Feb 2003–24 Oct 2003	867/905
ACE-FTS	9 Feb–25 March 2004	598/341



**Fig. 9.** Same as Fig. 8, but for MIPAS-STR flight at Kiruna, Sweden (68° N, 20° E) on 2 March 2003.

coincident measurements in the tropics, 67 in mid-latitudes and 665 in high-latitudes. In the low latitudes, the deviation is within  $\sim 0.3$  ppb or  $-10$  to  $+15\%$  at 20–34 km. The difference in the mid-latitudes is up to 1.4 ppb or 18%, whereas in the Arctic the difference between the profiles is up to 0.4 ppb or 3%, above 20 km. The mean MIPAS–ASUR deviation for the entire latitude band is up to 0.6 ppb or 10%. The MIPAS–ASUR difference is found to be largest in the mid latitudes and is lowest in the high latitudes with a peak around 23 km.

Beside the fact that the standard deviation of the differences for the predefined criterion (not shown) is greater than for the relaxed criterion, the shape of the delta profiles are alike in both analyses. It reveals that the largest deviation is in the 20–30 km region, where the MIPAS profiles generally exceed the ASUR profiles. Below 20 km, the ASUR values appear to be relatively small and thus give rise to large differences and high spread ( $1\sigma$  deviation of the values). The agreements between the profiles are very good above 30 km.

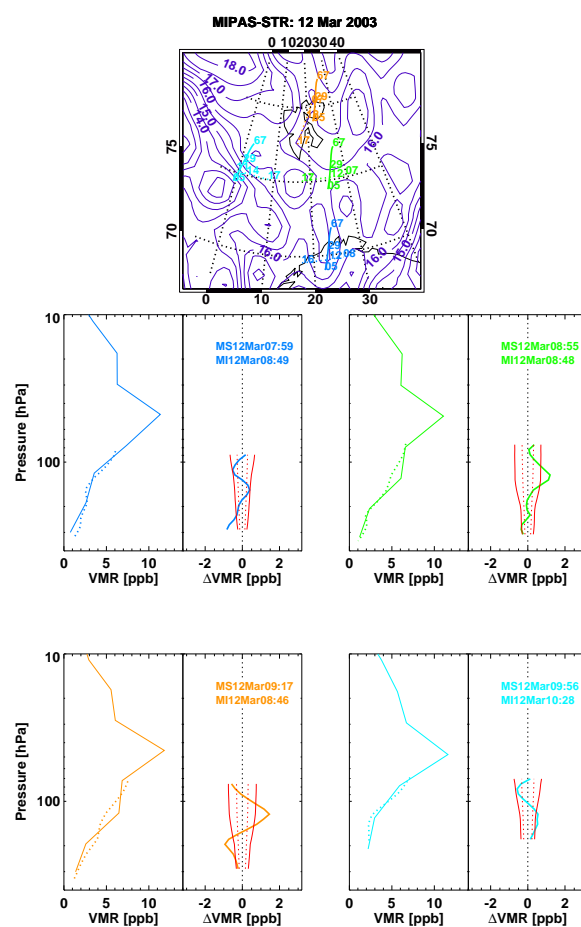


**Fig. 10.** Same as Fig. 8, but for MIPAS-STR flight at Kiruna, Sweden (68° N, 20° E) on 12 March 2003.

Nevertheless, the general overall agreement between the MIPAS and ASUR profiles is better than 10–13% at 20–34 km.

## 6 Comparisons with balloon-borne instruments

### 6.1 MIPAS-B

Balloon-borne observations are a very useful tool to obtain distributions of  $\text{HNO}_3$  with sufficiently high vertical resolution over most of the stratospheric altitude region. Three validation campaigns were carried out with MIPAS-B, the balloon-borne version of MIPAS (Friedl-Vallon et al., 2004) (see Table 6), whose vertical resolution is typically between 2 to 3 km. They were conducted on 24 September 2002, 20/21 March 2003, and 3 July 2003. Figures 13 to 15 show comparisons of  $\text{HNO}_3$  VMR profiles between the MIPAS/ENVISAT ESA retrieval and balloon-borne MIPAS-B measurements on 24 September 2002, 20/21 March 2003, and 3 July 2003, together with the satellite and balloon flight tracks. As shown

in Fig. 13, the two September MIPAS-B profiles were obtained from sequences measured near 40° N and 46° N on 24 September 2002. The MIPAS/ENVISAT coincident measurement for the sequence near 46° N covered nearly the same latitudes and longitudes along track of the flight while the sequence near 40° N is slightly different from the location of the MIPAS/ENVISAT observation. The two March 2003 measurements (Fig. 14) were taken in the late winter Arctic vortex near 66° N, 15° E over Kiruna (67.8° N, 20.4° E), Sweden and covered a wide range of longitudes (greater than 10°). The two sequences measured during the July flight (Fig. 15) were performed under polar summer conditions near 70° N around 10° E and 25° E with a longitudinal coverage of 10° to 15° respectively.

The agreement between ESA MIPAS and MIPAS-B HNO<sub>3</sub> profiles derived from the September radiance measurements at 40° N and 46° N is good (Fig. 13). During the northern sequence at 46° N the collocation was better than 20 min in time and better than 100 km in horizontal distance. The comparison between MIPAS-B (northern sequence) and MIPAS/ENVISAT reveals a good agreement with only slightly larger values of the MIPAS ESA data between 15 and 22 km (~130 and 50 hPa). The deviations are below 1 ppbv throughout the entire height range up to 38 km (~6 hPa), and below 0.5 ppbv above 26 km (~30 hPa). During the southern sequence at 40° N, the spatial mismatch between the MIPAS-B and MIPAS/ENVISAT measurements became slightly larger, and the difference of the measured HNO<sub>3</sub> VMR slightly increased, with a maximum of ~1.5 ppbv around the HNO<sub>3</sub> peak at 26 km (~30 hPa) and in the lower stratosphere at 18 km (~90 hPa). This difference is attributed to less perfect coincidence. However, parts of the disagreement can be attributed to some retrieval instabilities in the MIPAS profile measured at 22:05 UT exhibiting an unrealistic VMR double peak. Nevertheless, above 30 km (~17 hPa) no substantial difference between MIPAS and MIPAS-B HNO<sub>3</sub> profiles was found.

The HNO<sub>3</sub> profiles derived from the March flight at 66° N have shown larger differences of 1 to 3 ppbv between 17 and 22 km (~100 and 50 hPa) (Fig. 14). The discrepancies in the March measurements are attributed to horizontal inhomogeneities within a wide range of longitudes (larger than 10°) covered by MIPAS-B. Moreover, the March measurements were made near the vortex boundary (see violet contours in Fig. 14) where the variation of NO<sub>y</sub> species is highly pronounced due to differences in chemical processes on either side of the vortex edge. As shown by Mengistu Tsidu et al. (2005) the disagreements, which are more pronounced for HNO<sub>3</sub> than N<sub>2</sub>O<sub>5</sub>, are mainly caused by the horizontal inhomogeneity since HNO<sub>3</sub> exhibits a stronger latitudinal gradient than N<sub>2</sub>O<sub>5</sub>, particularly near the vortex edge.

In contrast, the HNO<sub>3</sub> profiles from the ESA MIPAS and MIPAS-B measurements near 70° N in July 2003 show better agreement, even the MIPAS-B July flight covered nearly the same wide longitude range, in comparison with the March

observations (Fig. 15). The deviations are less than 1 ppbv throughout the entire altitude range between 10 and 40 km (~260 and 4.5 hPa), and below 0.5 ppbv at the lower and higher altitudes. This reflects much smaller horizontal variations of the HNO<sub>3</sub> distributions during polar summer.

## 6.2 MkIV

Three balloon campaigns were made with the Jet Propulsion Laboratory (JPL) MkIV instrument (Toon, 1991) (see Table 6). It is a Fourier transform spectrometer and measures high signal-to-noise ratio solar occultation spectra throughout the mid-infrared region (650 to 5650 cm<sup>-1</sup>) at high spectral resolution (0.01 cm<sup>-1</sup>) at sunrise or sunset. Two sunrise MkIV measurements (Figs. 16 and 17) were taken over Esrange located 45 km from the town of Kiruna in 16 December 2002 and 1 April 2003 during SOLVE2/VINTERSOL campaigns (<http://mark4sun.jpl.nasa.gov/solve2a.html> and <http://mark4sun.jpl.nasa.gov/solve2b.html>). The December measurement has a wide latitude coverage while the April one extends over a wide longitude range. They have 3 and 4 coincident MIPAS/ENVISAT HNO<sub>3</sub> profiles, respectively. The third sunrise MkIV measurement (Fig. 18) was conducted in 20 September 2003 at a mid-latitude of 35° N with a wide longitude range. There are 6 coincident MIPAS/ENVISAT HNO<sub>3</sub> profiles available for this MkIV flight.

Figures 16 and 17 compare two sunrise MkIV measurements taken at high northern latitudes over Esrange during 2002 winter and 2003 spring with respect to their 3 and 4 coincident MIPAS/ENVISAT ESA profiles, respectively. The local time differences are small for these correlative profiles. Thus, their solar zenith angle differences are not adjusted.

The comparison of the December measurements (Fig. 16) shows substantial differences (e.g. zigzag in orange and blue curves), as large as ±(2 to 4) ppbv. Only the green curve, measured about one day earlier at similar latitudes shows a relatively good agreement with the MkIV result. A comparison with the HNO<sub>3</sub> results by the IMK-IAA data processor (see Wang et al., 2007, Fig. 4) shows that data below 24–25 km are not reported there for the orange and blue curves. The reason for this is that those tangent altitudes have been discarded from the IMK-IAA retrievals due to cloud contamination. These polar stratospheric clouds (PSCs) have not been detected with the ESA cloud index limit (Spang et al., 2004) but with the more stringent IMK index (Glatthor et al., 2006). Cloud-clearing is a general source of problems for all comparisons of ESA MIPAS trace gas retrievals at lower altitudes. In case of HNO<sub>3</sub>, which may be used to infer denitrification/uptake processes by polar stratospheric clouds in the polar stratosphere, it is especially important to exclude such erroneous retrievals by, e.g., checking the cloud index values. Thus, there are two explanations for the strong zigzag in the ESA results: 1) the profiles are correctly representing the gas-phase depletion of HNO<sub>3</sub> due to uptake into PSCs and possible denitrification/renitrification at lower altitudes,

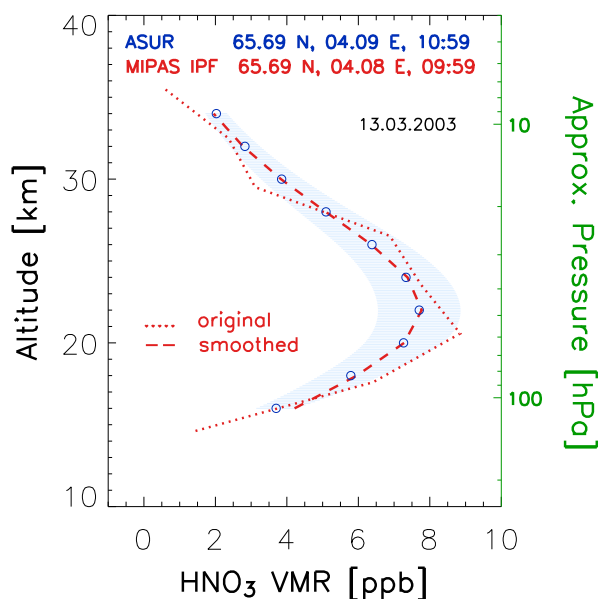


**Fig. 11.** A MIPAS and ASUR coincident measurement in the Arctic. Latitude, longitude, time and date of the measurements are noted in the figure. The shaded area indicates the estimated accuracy of the ASUR  $\text{HNO}_3$  retrieval. The MIPAS data convolved with the ASUR altitude resolution is indicated by the “smoothed” profile.

or 2) due to the interfering cloud signal the retrieval might have become unstable. We assume that both factors contribute to the observed profile shapes since 1) PSCs must have been present as indicated by the IMK-IAA cloud detection and, thus, an uptake of  $\text{HNO}_3$  is probable and 2) there is also a zigzag in the ESA retrieved MIPAS ozone profiles (not shown here) at the same geolocations as the orange and blue curves which is in phase with the zigzag of the  $\text{HNO}_3$  results, however, with an amplitude of about 20% compared to up to 70% in case of  $\text{HNO}_3$ . Since ozone is not known to be influenced directly by PSCs, we conclude that the observed instability is an artefact of the retrieval in presence of clouds.

In contrast, MIPAS and MkIV April  $\text{HNO}_3$  measurements (Fig. 17) are in reasonable agreement. The highest deviations in  $\text{HNO}_3$  VMR were found below 17 km ( $\sim 100$  hPa), with MkIV being 1.5 ppbv lower than ESA retrieved MIPAS  $\text{HNO}_3$  VMR. In the primary  $\text{HNO}_3$  VMR maximum around 23 km ( $\sim 45$  hPa) and above, deviations were around 0.5 ppbv.

The sunrise MkIV measurement at  $35^\circ\text{N}$  in September 2003 (Fig. 18) also show generally good agreement with its 6 coincident MIPAS/ENVISAT  $\text{HNO}_3$  profiles. The differences are less than 1.5 ppbv throughout the entire altitude range between 10 and 40 km ( $\sim 260$  and 4.5 hPa), and below 0.5 ppbv at the lower and higher ends. This is due

to more homogeneous airmasses at the autumn mid-latitude, though there was spatial mismatch of about  $10^\circ$  longitude between the coincident profiles. The forward trajectories started at the positions of the MkIV profile indicate that the turquoise MIPAS/ENVISAT profile measured on 18:29 UTC should agree best with the MkIV profile, as it represents the same air masses, which is the case indeed.

### 6.3 SPIRALE

The tunable diode laser instrument SPIRALE (Spectromètre Infra Rouge pour l'étude de l'Atmosphère par diodes Laser Embarquées) is a balloon-borne instrument for the in situ measurement of stratospheric trace species (Moreau et al., 2005). Concentrations of  $\text{O}_3$ ,  $\text{CO}$ ,  $\text{CO}_2$ ,  $\text{CH}_4$ ,  $\text{N}_2\text{O}$ ,  $\text{NO}_2$ ,  $\text{NO}$ ,  $\text{HNO}_3$ ,  $\text{HCl}$ ,  $\text{HOCl}$ ,  $\text{H}_2\text{O}_2$ , and  $\text{COF}_2$  have been retrieved from direct absorption in the mid-infrared spectral region by fitting experimental spectra and spectra calculated using spectroscopic parameters of absorption lines from the HITRAN2004 database (Rothman et al., 2005). Estimations of the uncertainties on SPIRALE measurements have been previously described in detail (Moreau et al., 2005). The global uncertainty on the  $\text{HNO}_3$  mixing ratio is estimated to be 30% below 20 km height mainly due to random errors and 20% above 20 km mainly due to systematic errors. The sources of random errors are the fluctuations of the laser background emission signal, and the low signal-to-noise ratio for weakly absorbing species such as  $\text{HNO}_3$ . The sources of systematic errors are on the laser linewidth (an intrinsic characteristic of the diode laser) and on the non-linearity of the detectors. It is to be noted that systematic errors on spectroscopic data (essentially molecular line strength and pressure broadening coefficients) are not considered.

Validation flights were carried out from Aire sur l'Adour, France ( $43.7^\circ\text{N}$ ,  $0.3^\circ\text{E}$ ) on 2 October 2002 and from Kiruna, Sweden ( $67.8^\circ\text{N}$ ,  $20.4^\circ\text{E}$ ) on 21 January 2003. MIPAS  $\text{HNO}_3$  operational data have been compared with the SPIRALE profiles obtained during the descent phase of the October 2002 flight and during the ascent phase of the January 2003 flight.

Figure 19 shows comparisons of the  $\text{HNO}_3$  profiles obtained by SPIRALE during the Kiruna 2003 flight. For the Arctic flight, direct coincidences with two MIPAS scans (orbit 4677-scan 20 and orbit 4678-scan 6), whose temporal separation from the SPIRALE measurements satisfied the baseline matching criterion  $\Delta t < 3$  h, were available. The location of this flight was close to the vortex edge and, although the spatial separation does not satisfy the baseline criterion  $\Delta s < 300$  km (300–500 km for scan 20 and 600–800 km for scan 6), MIPAS and SPIRALE measurements were made on locations where PV computed by the contour advection model MIMOSA (Hauchecorne et al., 2002) were close (5 to 25% for scan 20 and 5 to 35% for scan 6). Both the SPIRALE original high vertical resolution profile and its smoothed version after application of MIPAS averaging

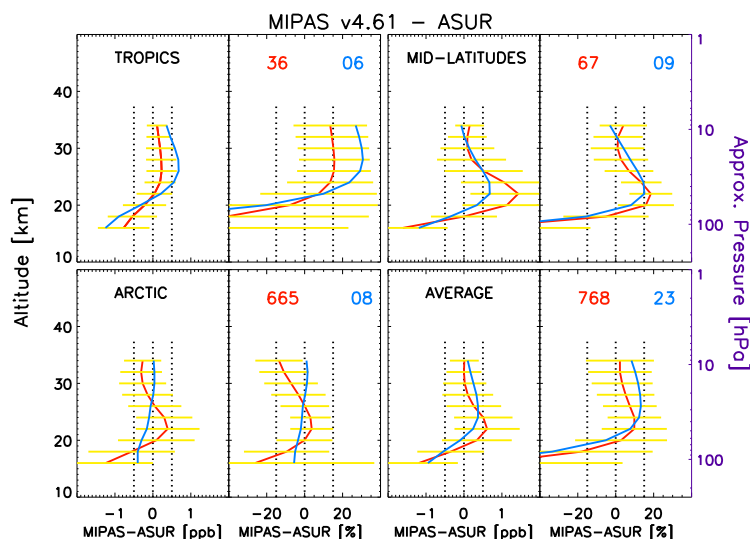


**Fig. 12.** The statistics derived from the MIPAS-ASUR nitric acid profiles at different latitude regions together with the mean difference for all latitude regions. The blue curves stand for the predefined criterion of 300 km and 3 h and the red curves stand for the analyses with the additional criterion of 1000 km and 12 h. The yellow bars on the red curves show the 1- $\sigma$  deviation of the delta profiles. The numbers on the plots indicate the respective number of coincident measurements at each latitude section for the respective analysis. Dotted black lines indicate values of  $-0.5$ ,  $0$ , and  $0.5$  ppbv and  $-15$ ,  $0$ , and  $15\%$ , respectively.

kernels are displayed. In general, a good agreement is observed in both cases, with MIPAS  $\text{HNO}_3$  data from orbit 4677, scan 20 mostly matching SPIRALE smoothed values within the error bars. Discrepancies which can reach 4 ppbv at the level above 100 hPa, are found in the comparison with MIPAS orbit 4678, scan 6, possibly due to increased comparison errors introduced by the greater spatial separation (600–800 km) and by the large PV differences at the level above 100 hPa (35%).

Figure 20 shows comparisons of the  $\text{HNO}_3$  profiles obtained by SPIRALE on the October 2002 flight with coincident MIPAS profiles from orbit 3019, scans 14 and 15 on 27 September at 23:52:50 UT and 23:54:11 UT respectively. For the mid-latitude flight, direct coincidences satisfying the criteria of  $\Delta t < 3$  h and  $\Delta s < 300$  km where not possible, and the intercomparison was carried out by means of trajectory analysis with MIPAS profiles. The backward trajectories ending at the location of the SPIRALE profiles ( $44^\circ$  N,  $0^\circ$  E) on 2 October 2002 (09:15–10:30 UT at descent) have been computed as a function of potential temperature in 25 K steps (about 1 km). Scans 14 and 15 of orbit 3019 have been proven to be the best matches for comparison with SPIRALE. These scans were measured near  $42^\circ$  N and  $46^\circ$  N, 4.5 days before the SPIRALE flight. By comparing the PV values of SPIRALE and MIPAS profiles, it is found that PV differences are lower than 10% between 400 K and 600 K for both MIPAS scans and above 700 K for scan 14. This concludes that the SPIRALE data may be used to validate 1) MIPAS scan 14 of orbit 3019 on the potential

surfaces between 400 K and 600 K and between 700 K and 900 K, which corresponds to the retrieval nominal MIPAS altitudes 18, 21, 24, 30 and 33 km, and 2) MIPAS scan 15 of orbit 3019 on the potential surfaces between 400 K and 600 K, which corresponds to the nominal MIPAS altitudes: 18, 21 and 24 km. The comparison results shown in Fig. 20 reveal a generally good overlapping between MIPAS and SPIRALE  $\text{HNO}_3$  measurements, except for the altitudes near the VMR peak (21 and 24 km) where the MIPAS data overestimate the SPIRALE observations by 2 ppbv at 21 km for both MIPAS scans and by 3 ppbv at 24 km for MIPAS scan 15. In the latter case large differences on the PV values of SPIRALE and MIPAS profiles above 24 km (35% at 27 km, 60% at 30 km) could explain the discrepancies since MIPAS retrieved mixing ratios at a nominal tangent altitude depends on the true mixing ratio values at least within the half width of the vertical field-of-view above. Further, inspecting MIPAS  $\text{HNO}_3$  profiles of orbit 3019 further north (not shown here) reveals a strong S-N gradient at the altitude of the largest differences (30–40 hPa) compared to SPIRALE. This strong gradient is the result of a PV barrier close to SPIRALE and to MIPAS scan 15. Considering the time difference of 4.5 days small errors on the ECMWF (European Centre for Medium-range Weather Forecasts) winds could lead to small errors on the location of the PV barrier close to MIPAS or close to SPIRALE (or both) leading to larger errors on the PV differences between the locations of SPIRALE and MIPAS.

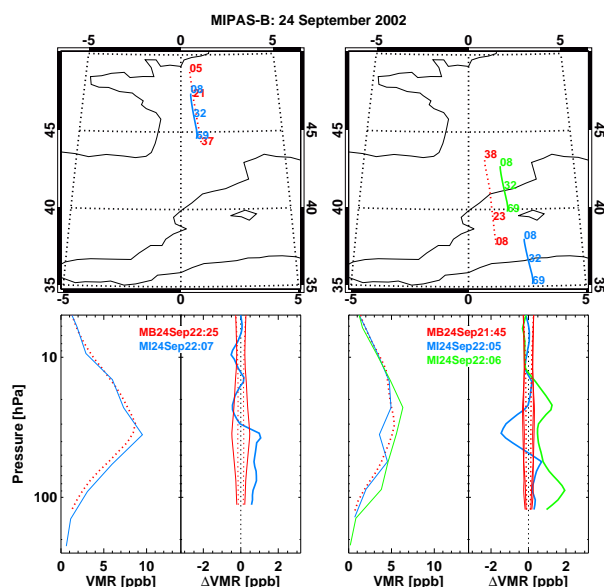


**Fig. 13.** Comparison of  $\text{HNO}_3$  volume mixing ratio (in ppbv) profiles observed by MIPAS-B (red dotted) and MIPAS/ENVISAT (other colors) on 24 September 2002. The top panels show the balloon flight and satellite tangent point tracks for the MIPAS-B northern (left) and southern (right) measured sequences. The numbers indicate the altitudes (in kilometers) of selected tangent points. All measurements were located outside the polar vortex, and thus the contour lines of potential vorticity are not shown. The bottom panels show the profiles (the first and third column from the left) and their differences (the second and fourth column). In the difference panels, the combined noise error is red dotted and the combined total error (without errors from HITRAN) is red solid.

#### 6.4 IBEX

IBEX (Infrared Balloon EXperiment) is a high resolution Fourier transform spectrometer operating in the Far-IR region (spectral range  $10\text{--}250\text{ cm}^{-1}$ , spectral resolution  $0.0025\text{ cm}^{-1}$ ) for limb emission measurements from stratospheric balloon (Bianchini et al., 2006). The correlative measurements with MIPAS/ENVISAT were obtained during the trans-Mediterranean flight from Trapani, Sicily ( $38^\circ\text{ N}$ ,  $12^\circ\text{ E}$ ) to Spain on 29–30 July 2002. However, useful coincidences between MIPAS observations and measurements of the FT-FIR spectrometer could be obtained only after substantial relaxation of the spatial-temporal matching criteria (within 300 km and 3 h), as shown for instance in previous analyses carried out for MIPAS ozone validation (Cortesi et al., 2004). As a consequence, the comparison of MIPAS and IBEX data was based on isentropic trajectories calculations performed using the University of L'Aquila Global Trajectory Model (Redaelli, 1997; Dragani et al., 2002) on the base of ECMWF meteorological fields. Four days backward and forward isentropic trajectories, departing from the

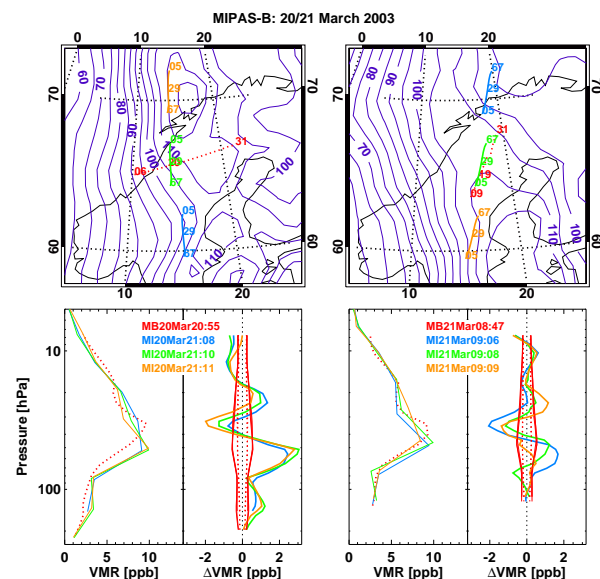


**Fig. 14.** Same as Fig. 13, but for two MIPAS-B sequences measured on 20/21 March 2003. Overlaid violet contour lines are potential vorticity (in  $10^{-6}\text{ K m}^2\text{ kg}^{-1}\text{ s}^{-1}$ ) at 550 K potential temperature.

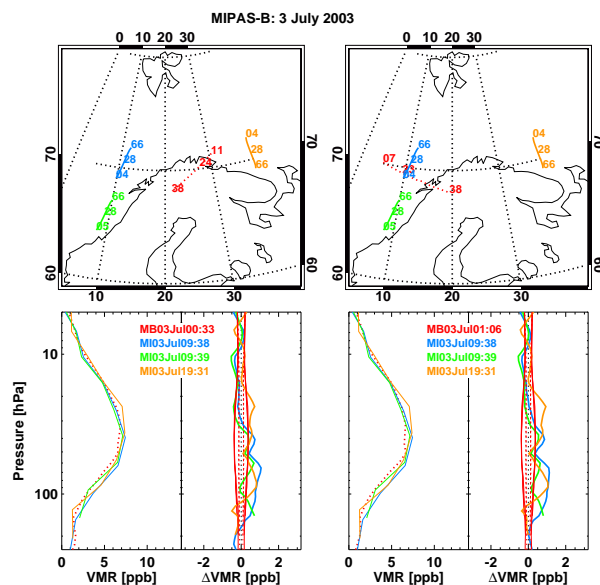


**Fig. 15.** Same as Fig. 13, but for two MIPAS-B sequences measured on 3 July 2003.

geolocations of the IBEX retrieved profiles, were calculated. Then MIPAS  $\text{HNO}_3$  profiles at locations within 2 degrees in longitude, 2 degrees in latitude and 2 h in time along these trajectories were identified and vertically interpolated in potential temperature, to obtain the  $\text{HNO}_3$  volume mixing ra-

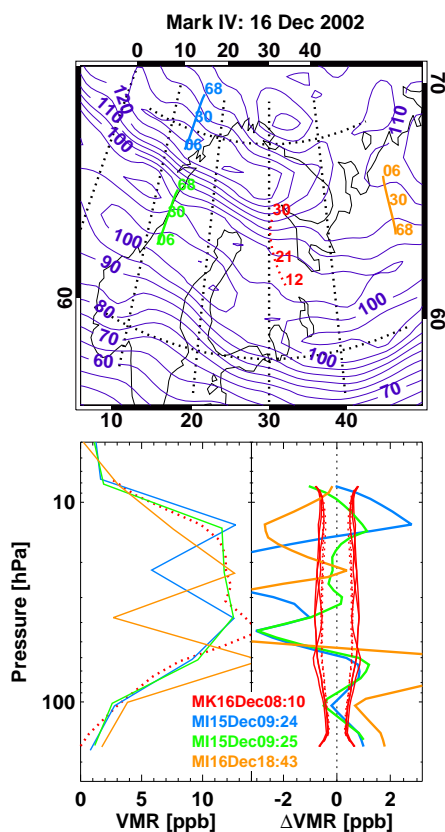


**Fig. 16.** Comparison of  $\text{HNO}_3$  volume mixing ratio (in ppbv) profiles observed by MkIV (red dotted) and MIPAS/ENVISAT (other colors) on 16 December 2002. The top panel shows the balloon flight and satellite tangent point tracks. The numbers indicate the altitudes (in kilometers) of selected tangent points. The bottom panel shows the profiles (left) and their differences (right). In the difference panels, the combined noise error is red dotted and the combined total error (without errors from HITRAN) is red solid. Overlaid violet contour lines are potential vorticity (in  $10^{-6} \text{ K m}^2 \text{ kg}^{-1} \text{ s}^{-1}$ ) at 550 K potential temperature.

tio value to be compared with the corresponding MIPAS measurements. The interpolation to the trajectories has been made by using the pressures of MIPAS as height coordinate and not the altitudes. The resulting intercomparison pairs were then binned by altitude, in steps of  $\Delta z=1.5$  km and averaged. Preliminary results of a so called “self-hunting” analyses of MIPAS data that matches satellite observation with themselves, providing a test for the precision of the instrument products and the quality of the calculated trajectories and thus assessing the noise in the technique and providing estimates to its possible extension to multi-platform comparison for the selected time period, can be found in Taddei et al. (2006).

Mean absolute and relative differences between the MIPAS and IBEX  $\text{HNO}_3$  data obtained during the trans-

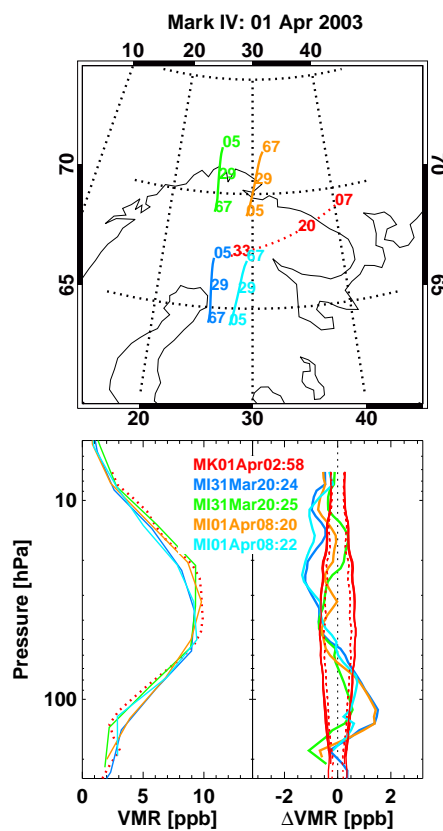


**Fig. 17.** Same as Fig. 16, but for MkIV flight on 1 April 2003. All measurements were located outside the polar vortex, and thus the contour lines of potential vorticity are not shown.

**Table 7.** Mean spatial and temporal separations and standard deviations. Data are averaged over all available correlative measurements (see Table 6). Horizontal distance in kilometers, latitude and longitude in degrees, and time in minutes (note: Both daytime and nighttime MIPAS measurements are used for comparison with ACE-FTS data).

	Odin/SMR	ILAS-II	ACE-FTS
Distance	$197 \pm 69$	$208 \pm 68$	$280 \pm 151$
Latitude	$-0.5 \pm 1.2$	$-0.1 \pm 1.4$	$1.5 \pm 1.9$
Longitude	$-0.02 \pm 8.3$	$-0.6 \pm 6.9$	$11.3 \pm 43.3^*$
Time	$27 \pm 105$	$22 \pm 114$	$426 \pm 504^*$

Mediterranean flight of 29–30 July 2002 are presented in Fig. 21. The MIPAS measurements agree reasonably well with the balloon profile between 17 and 32 km (mean relative differences within  $\pm 15\%$ ). However, at lower and higher altitudes, MIPAS  $\text{HNO}_3$  VMRs appear to be higher than those of the IBEX by up to 50–100%.

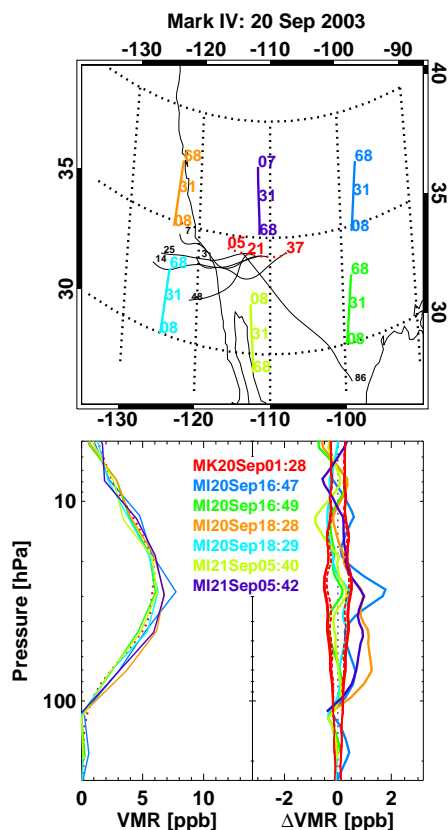


**Fig. 18.** Same as Fig. 16, but for MkIV flight on 20 September 2003. All measurements were located outside the polar vortex, and thus the contour lines of potential vorticity are not shown. The black lines are forward trajectories started from the position of the MKIV profile and all MIPAS observations took place afterwards.

## 7 Comparisons with other satellite observations

For comparisons of MIPAS with Odin/SMR and ILAS-II measurements, the horizontal separations between the collocated profiles are required to be smaller than 300 km, and the time differences are less than 3 h. However, for ACE-FTS, due to limitations of satellite's sampling and database size, 800 km, 9 h and a maximum difference of potential vorticity of  $3 \times 10^{-6} \text{ Km}^2 \text{ kg}^{-1} \text{ s}^{-1}$  at an altitude of 475 K potential temperature are used to obtain enough coincidences for statistical analysis. The numbers of available coincident profiles are listed in Table 6. The mean spatial separations and temporal differences, as well as their standard deviations are averaged over all available correlative measurements and listed in Table 7. The spatial and temporal mismatch can cause  $\text{HNO}_3$  differences associated with geophysical variations of the atmospheric field. However, imperfect spatial/temporal matches have virtually no effect on the observed mean differences since their effect largely averages out, but may significantly contribute to the observed

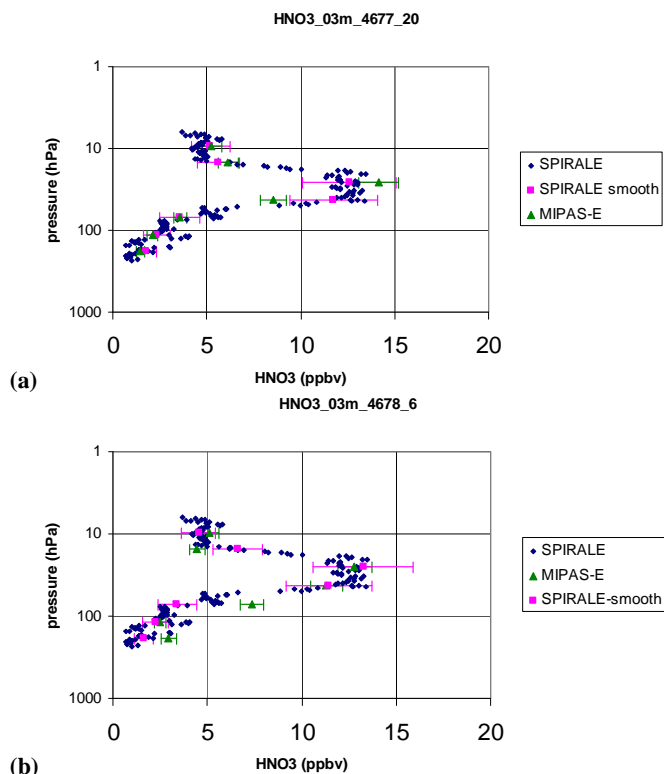


**Fig. 19.** Comparison between MIPAS ESA operational and SPIRALE  $\text{HNO}_3$  measurements at Kiruna, Sweden on 21 January 2003. Error bars represent total (systematic plus random) MIPAS and SPIRALE uncertainties.

standard deviations. This has been confirmed by re-analysis of the Odin/SMR and ILAS-II data using much less restricted criteria, which require the latitude and longitude separations being smaller than 5 and 10 degrees, respectively, and the time differences less than 12 h (The results are not shown here).

For a reference data set having enough correlative profiles, mean differences at individual height levels are also calculated over the overlapped observation period. For inter-satellite comparison, zonal mean differences are calculated with latitude intervals of  $30^\circ$  and for the MIPAS descending (daytime) and ascending (nighttime) orbit nodes separately. The results from both nodes are generally similar and thus combined together. The global means are averaged over all latitudes and both orbit nodes.

### 7.1 Odin/SMR

The Sub-Millimetre Radiometer (SMR) on board the Odin satellite, launched on 20 February 2001, observes key species with respect to stratospheric chemistry and dynamics such as  $\text{O}_3$ ,  $\text{ClO}$ ,  $\text{N}_2\text{O}$ , and  $\text{HNO}_3$  using two bands centered at 501.8 and 544.6 GHz. Stratospheric mode measurements are

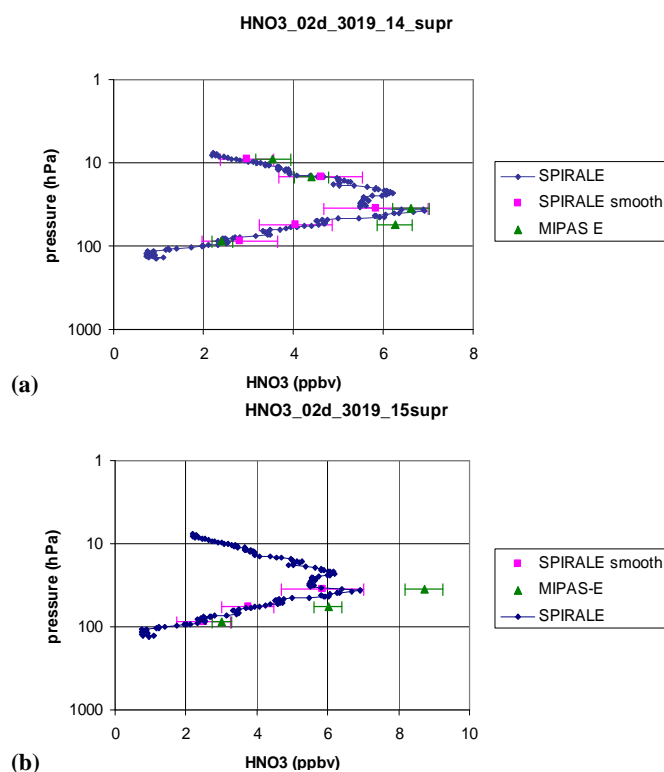


**Fig. 20.** Comparison between MIPAS ESA operational and SPIRALE  $\text{HNO}_3$  measurements at Aire sur l'Adour, France on 2 October 2002. Error bars represent total (systematic plus random) MIPAS and SPIRALE uncertainties.

performed typically twice per week. Vertical profiles are retrieved from the spectral measurements of a limb scan by two similar data processors in Sweden and in France. The data used in this comparison study are taken from the level 2 operational data retrieved at the Chalmers University of Technology (Gothenburg, Sweden). The most recent version is version 2.0, and  $\text{HNO}_3$  is retrieved from the 544.6 GHz band. The profiles in the altitude range from 18 to 45 km are retrieved with a vertical resolution of 1.5 to 2 km and a  $1\text{-}\sigma$  precision of better than 1.5 ppbv. In the height regions below  $\sim 18\text{--}20$  km ( $\sim 88\text{--}67$  hPa), the Odin/SMR  $\text{HNO}_3$  data usually have a measurement response (a ratio derived from the Odin/SMR averaging kernel matrix and providing a measure on how much information comes from the spectral measurement and the a priori profile for each individual retrieval altitude level) lower than 0.75, implying dominance of the a priori climatology. Thus, we select data with the measurement response larger than 0.75 for comparison. Detailed information on the data characteristics and analysis of systematic retrieval errors, resulting from spectroscopic and instrumental uncertainties can be found in Urban et al. (2005) and Urban et al. (2006).

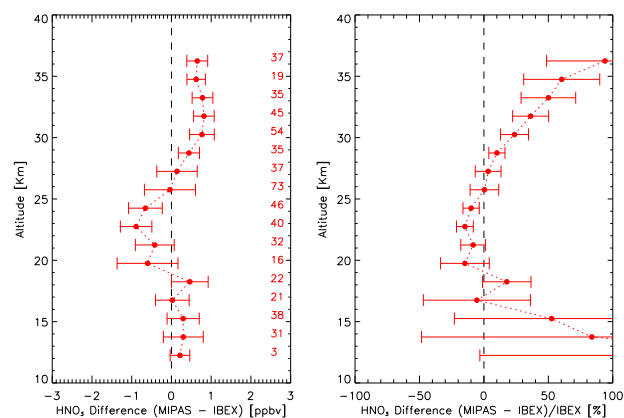


**Fig. 21.** Comparison between MIPAS ESA operational and IBEX (29–30 July 2002)  $\text{HNO}_3$  measurements. Mean absolute (left) and relative (right) differences between MIPAS and IBEX  $\text{HNO}_3$  VMR were reconstructed using trajectory analysis and averaged in altitude bins of  $\Delta z = 1.5$  km. Error bars represent  $1\text{-}\sigma$  standard deviations. The number of elements per altitude bin is also displayed.

Comparison between the MIPAS IMK-IAA and Odin/SMR  $\text{HNO}_3$  data by Wang et al. (2007) has shown that the characteristic shape of the difference profile likely indicate an altitude shift in the SMR profiles, and the best value of the mean altitude increase for Odin/SMR, which minimizes the  $\text{HNO}_3$  VMRs differences was estimated to be approximately 1.5 km. Therefore, the altitudes of Odin/SMR data have been increased by 1.5 km, and the retrieved pressures have been adjusted by interpolating the original altitude-pressure scales to the adjusted heights. The adjusted retrieved pressure values are used in this analysis.

Figure 22 shows the comparisons between the ESA retrieved MIPAS and Odin/SMR  $\text{HNO}_3$  VMR profiles, which are zonally averaged for 3 latitude bands during a period of 37 days from 19 September 2002 to 28 February 2003. No coincident measurement is available between  $30^\circ$  N and  $60^\circ$  S due to our requirement of the horizontal separation  $< 300$  km, more restricted than that used by Wang et al. (2007). The comparison results are consistent with preliminary results obtained from the Odin/SMR validation study based on comparisons of Odin/SMR with a couple of balloons and with satellite data (ILAS-II, MIPAS ESA operational data) (Urban et al., 2006).

The Odin/SMR  $\text{HNO}_3$  version 2.0 data used in this analysis show good agreement with the correlative data. Their differences at the three latitude bands and the overall means averaged over these bands (not shown) are generally smaller than the combined measurement errors of both instruments in the altitude range above 30 km ( $\sim 17$  hPa), and slightly larger below 30 km. The Odin/SMR VMRs tend to be larger than those of the MIPAS by 10–20% (1–2 ppbv) in the altitude

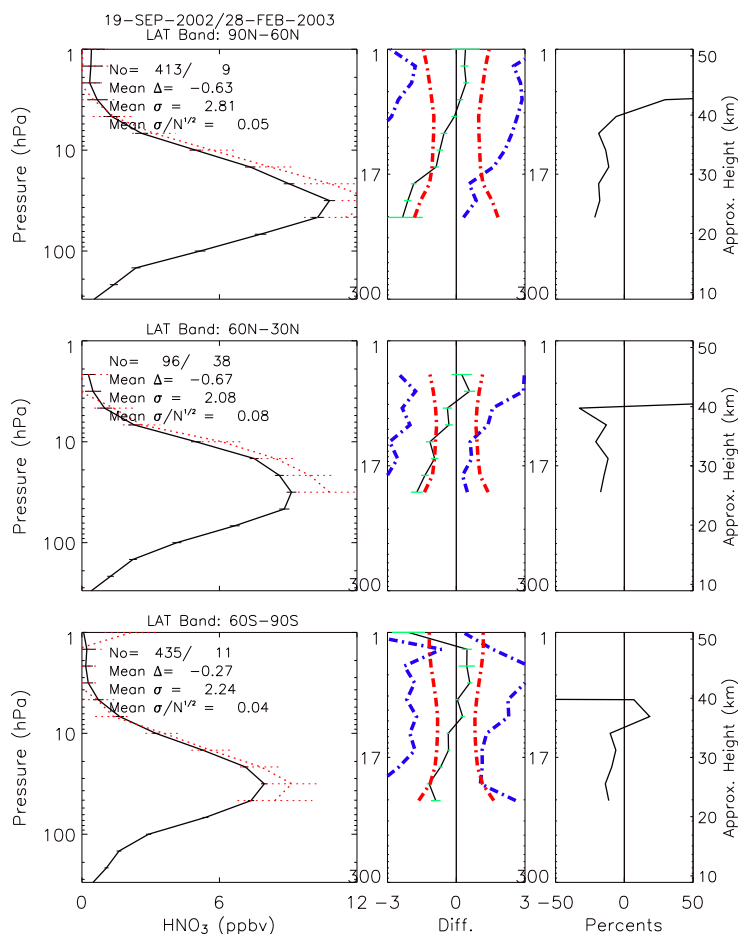


**Fig. 22.** Comparison of the ESA-operational MIPAS and Odin/SMR  $\text{HNO}_3$  volume mixing ratio (in ppbv) profiles at latitudes of  $60^\circ\text{N}$ – $90^\circ\text{N}$ ,  $30^\circ\text{N}$ – $60^\circ\text{N}$ , and  $60^\circ\text{S}$ – $90^\circ\text{S}$  during a period of 37 days between 19 September 2002 to 28 February 2003. The zonal mean profiles (left) are derived from the available coincident MIPAS (black solid) Odin/SMR (red dotted) measurements, which are located within a latitude interval of  $30^\circ$ . ODIN pressures have been adjusted according to an upward shift of the profiles by 1.5 km (see text for details). Shown in middle columns are the MIPAS minus Odin/SMR residuals (black), their standard deviations (blue dashed) and 1- $\sigma$  uncertainty (green bar), and estimated combined errors (red dashed) in ppbv. The estimated combined error is the mean of quadratically combined MIPAS and Odin/SMR total (systematic plus random) errors. The relative differences (right) are calculated with respect to a mean profile averaged over the MIPAS and Odin/SMR data. The maximum and minimum number of profiles available at individual heights are specified. Also denoted are the mean difference  $\Delta$ , standard deviations  $\sigma$ , and the uncertainty  $\sigma/\sqrt{N}$  averaged over all heights, where  $N$  is total number of available data points.

range 20–35 km, depending on latitude. Largest difference are found at high northern latitudes (up to 2 ppbv or 20% at 20–25 km), otherwise the agreement is within 1 ppbv or 10%. This indicates that the altitude shift is not the only reason for the disagreement, and other error sources (spectroscopy, calibration) may also contribute. Also, we note that a correction of 1.5 km looks too large in one of the chosen latitude bands ( $60^\circ$  to  $90^\circ\text{N}$ ), but very reasonable in the others, suggesting a possible latitude dependence of the altitude shift.

The standard deviations of the difference residuals (2–4 ppbv or more) shown in Fig. 22 are always larger than the combined measurement error. This is probably due to

the temporal and spatial coincidence error and the horizontal smoothing error which are not taken into account in our error budget (see Sect. 4). Also, it is worth noting that the standard deviations are larger (by 1 ppbv or more) than those of the MIPAS IMK-IAA retrievals with respect to the Odin/SMR data (see Wang et al., 2007, Figs. 8–10), in spite of much less restricted coincidence criteria used for the IMK-IAA data. The higher standard deviations in the operational dataset come likely from the effects of undetected clouds and different regularization used for the MIPAS ESA and IMK-IAA retrievals (see Sect. 6.2).

## 7.2 ILAS-II

The ILAS-II instrument is a solar occultation sensor designed to measure various stratospheric constituents. The operational observations were made with a frequency of about 14 times per day in each hemisphere for about 7 months from 2 April through 24 October 2003. The measurement latitudes ranged from 54° to 71° N and from 65° to 88° S, varying seasonally. Vertical profiles of HNO<sub>3</sub> and several key stratospheric species (O<sub>3</sub>, NO<sub>2</sub>, N<sub>2</sub>O, CH<sub>4</sub>, H<sub>2</sub>O etc.) are simultaneously retrieved by the so-called onion-peeling method, primarily using the strong absorption lines around 7.6 and 11.3 μm for the HNO<sub>3</sub> retrieval, with vertical resolutions of 1.3 to 2.9 km at tangent heights of 15 and 55 km (see Yokota et al., 2002, for details of the retrieval algorithm cloud-clearing technique). For altitude registration, the geometric altitude data are obtained from the sun-edge sensor. However, the pressure/temperature (p/T) data of the ILAS-II retrievals are not good in accuracy (Sugita et al., 2004). Thus, the assimilation analysis data (registered in geopotential altitude) from the Met Office (METO, also previously referred to as UKMO), United Kingdom are converted to get the interpolated T/p profiles. This choice is a continuation from ILAS experiment. However, to facilitate comparisons of HNO<sub>3</sub> in this study, we obtain the p/T profiles from the ECMWF assimilation, which is used to derive the hydrostatic pressure profiles in the MIPAS data retrievals. For the version 1.4 ILAS-II algorithm, spectroscopic data were adopted from the HITRAN2000 database, including updates through the end of 2001 (Rothman et al., 2003). The influence of the different version of HITRAN database (2000 versus 2004) on ILAS-II HNO<sub>3</sub> retrievals is very small, according to a sensitivity test made for a couple of specific cases. The ILAS-II stratospheric HNO<sub>3</sub> profiles (version 1.4) were validated with balloon-borne instruments and climatological comparisons, showing that the precision is better than 13–14%, 5%, and 1% at 15, 20, and 25 km, respectively, and that the accuracy in the altitude region is estimated to be better than –13% to +26% (Irie et al., 2006; Yamamori et al., 2006).

Figure 23 shows comparisons between the ESA retrieved MIPAS and ILAS-II measured HNO<sub>3</sub> VMR profiles, which are zonally averaged over three latitude bands for the 82 days between 12 February to 24 October 2003. No coincident measurement is available in other latitude bands. The ILAS-II data were convolved with the MIPAS averaging kernel. Therefore, the ILAS-II mixing ratios are somewhat degraded from the original vertical resolutions. Also, the ILAS-II data were filtered by requiring the retrieved VMR values greater than the total error values. This rejected some data points above about 35 km (~9 hPa), in particular, in the southern high latitude region.

The consistency between the MIPAS and ILAS-II data is very impressive, with the mean differences at individual latitude bands and averaged over the three bands (not shown) being less than the combined measurement errors of both in-

struments in the whole altitude range of 10 to 50 km. The 82-day mean differences being less than ±0.5 ppbv between 10 and 45 km (~260 and 2.3 hPa) and the standard deviations 1–2 ppbv. As seen from Fig. 23, the standard deviations are generally comparable to or smaller than the combined instrument measurement errors, except for the southern polar region around 20 km. Also, vertical trends in the difference between MIPAS and ILAS-II are different for the two hemispheres, with the ILAS-II data larger than the MIPAS at the height levels below the VMR peak in the southern polar region. These features are probably due to the same reasons for other comparisons (see Sects. 4 and 7.1): the coincidence of sounding airmasses and the horizontal smoothing errors are not taken into account in the error budget. Both errors become large in the southern polar region where the spatial variability of target molecule is high. On a first instance, the good consistency between ILAS-II and MIPAS is surprising, since different spectroscopic data (HITRAN2000 for ILAS-II and HITRAN2004 for MIPAS) are used in the retrievals. A possible explanation, arising from the additional absorption band used for the ILAS-II retrieval, is given in Wang et al. (2007).

## 7.3 ACE-FTS

The ACE-FTS (Bernath et al., 2005) is a high resolution (0.02 cm<sup>-1</sup>) Fourier transform spectrometer operating from 2 to 13 μm (750 to 4500 cm<sup>-1</sup>). The ACE-FTS records atmospheric absorption spectra during sunrise and sunset (solar occultation mode) and has a nominal vertical resolution of about 4 km. The ACE satellite was launched on 12 August 2003 and the first useful atmospheric spectra were recorded in early February 2004. The ACE-FTS retrieval algorithm is based on a global fit procedure that first derives temperature and pressure profiles using CO<sub>2</sub> absorption (Boone et al., 2005). The nitric acid is based primarily on microwindows near 1710 cm<sup>-1</sup> containing ν<sub>2</sub> absorption. In the troposphere additional microwindows near 879 cm<sup>-1</sup> (ν<sub>5</sub>) are used because of strong water absorption near the ν<sub>2</sub> band. The HNO<sub>3</sub> line parameters used are those of HITRAN 2004 (Rothman et al., 2005). Version 2.2 FTS retrievals taken during 9 February to 25 March 2004 are used for the comparisons in this paper. The retrievals are carried out in the 10 to 37 km range with a typical precision of 2 to 3%.

Figure 24 shows comparisons between the zonal mean profiles of the ESA MIPAS and ACE-FTS HNO<sub>3</sub> VMR taken during 9 February to 25 March 2004 at latitude bands of 30° N–60° N and 60° N–90° N. The ACE-FTS data are from the sunset measurements, while the MIPAS data include both daytime and nighttime measurements. The consistency between the MIPAS and ACE-FTS data is very good. The mean differences are less than ±0.1 to 0.5 ppbv and rms deviations of ~0.6 to 1 ppbv, with the smaller values corresponding to the lower and higher altitudes around 10 and 35 km (~260 and 9 hPa). The relative differences are

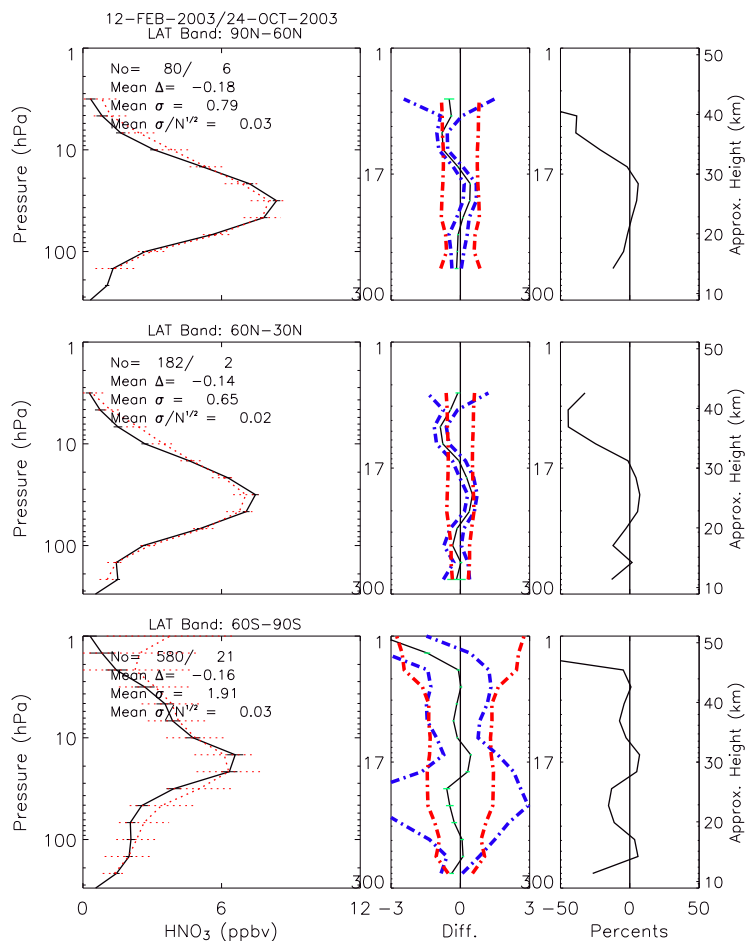


**Fig. 23.** Same as Fig. 22, but for comparison of the ESA-operational MIPAS and ILAS-II HNO<sub>3</sub> volume mixing ratio (in ppbv) profiles during a period of 82 days between 12 February to 24 October 2003. The ILAS-II data are convolved with the MIPAS averaging kernel.

5 to 10% below 30 km ( $\sim 17$  hPa), and 10 to 15% at higher altitudes around 35 km ( $\sim 9$  hPa). We have also compared the ACE-FTS sunset data with the daytime and nighttime MIPAS measurements separately, and no significant differences are found. For latitude bands of  $30^\circ$  S– $0^\circ$  and  $0^\circ$ – $30^\circ$  N, only 1 and 4 events are available respectively. Thus these comparison results are not presented here.

## 8 Conclusions

Stratospheric nitric acid VMR profiles are retrieved by ESA from the MIPAS observations using the operational data processor. The profiles of version v4.61/4.62 obtained between July 2002 and March 2004 are validated in this paper by comparing with a number of ground-based measurements, balloon and aircraft campaigns, and satellite observations.

The ESA MIPAS HNO<sub>3</sub> data show generally good agreement with various ground-based, balloon, and aircraft mea-

surements. The mean relative differences of HNO<sub>3</sub> partial columns between the MIPAS and FTIR at five stations are within  $\pm 2\%$ , which is the MIPAS systematic error for the partial columns, and the statistical standard errors on the means are 6–11%. The bias between the MIPAS and FTIR vertical profiles is statistically insignificant and below 10% with the statistical standard deviations of the mean differences of 5–13%. The aircraft-borne SAFIRE-A HNO<sub>3</sub> and MIPAS-STR measurements are generally matched with the satellite data within their total error bars. The general overall agreement between the MIPAS and ASUR profiles is better than 10–13% at 20–34 km. The largest deviation is in the 20–30 km region, where the MIPAS profiles generally exceeded the ASUR profiles. All differences for the comparison with balloon-borne MIPAS-B in September 2002 are below 1 ppbv throughout the entire altitude range up to about 38 km ( $\sim 6$  hPa), and below 0.5 ppbv above 30 km ( $\sim 17$  hPa). Similar features are also observed in comparisons between individual profiles of the MkIV and MIPAS/ENVISAT in April

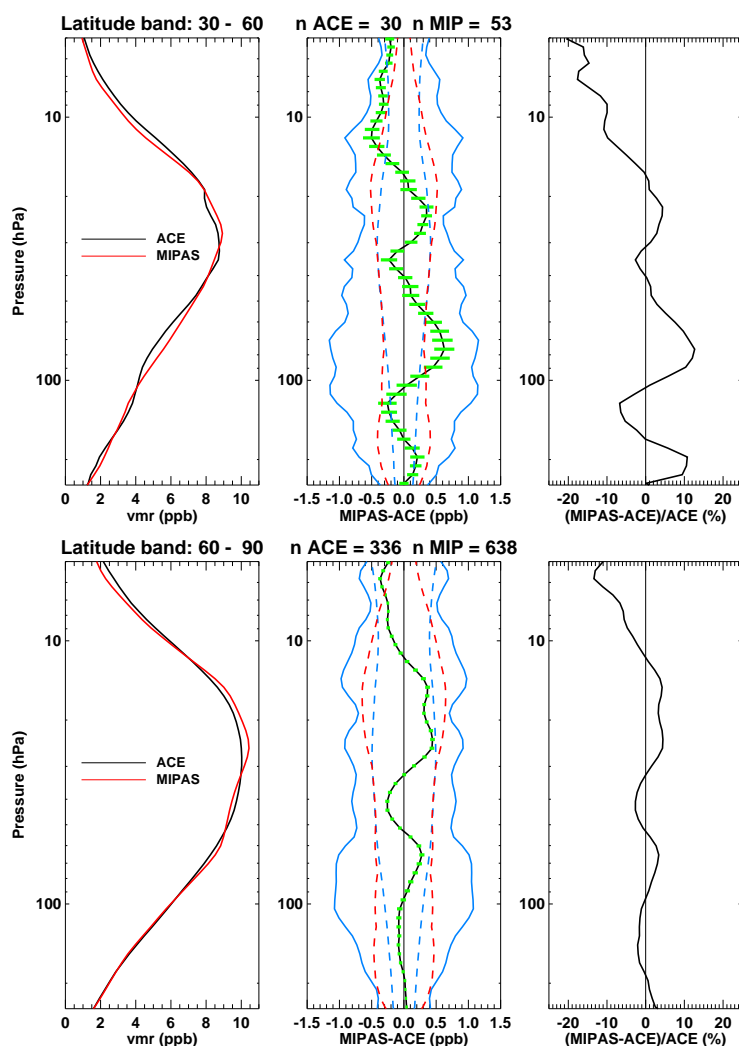


**Fig. 24.** Comparison of the ESA-operational MIPAS and ACE-FTS  $\text{HNO}_3$  volume mixing ratio (in ppbv) profiles at latitudes of  $30^\circ\text{N}$ – $60^\circ\text{N}$  and  $60^\circ\text{N}$ – $90^\circ\text{N}$  during 9 February to 25 March 2004. The zonal mean profiles (left) are derived from the available coincident MIPAS (red) and ACE-FTS (black) measurements, which are located within a latitude interval of  $30^\circ$ . Shown in middle panels are the MIPAS minus the ACE-FTS residuals (black), their standard deviations (blue) and  $1\text{-}\sigma$  uncertainty (green bar), estimated combined random error (blue dashed), and MIPAS systematic error (red dashed) in ppbv. The estimated combined random error is the mean of combined ACE-FTS and MIPAS noise errors where the MIPAS temperature error was added (quadratically) to the MIPAS noise errors. The MIPAS systematic error includes the HITRAN error, but without the temperature error. The relative differences (right) are calculated with respect to the ACE-FTS profiles. The total number of profiles is specified in the title.

2003. In the primary  $\text{HNO}_3$  VMR maximum around 23 km ( $\sim 45$  hPa) and above, deviations were around 0.5 ppbv. The MIPAS  $\text{HNO}_3$  data are also mostly matching balloon-borne SPIRALE values within the combined instrument error bars (the largest bias is less than 1 ppbv), when the location of the SPIRALE measurement is closer to that of MIPAS ( $\Delta s < 300\text{--}500$  km, and  $\Delta PV < 5$  to 25%). The MIPAS measurements agree reasonably well with the balloon IBEX profiles between 17 and 32 km (mean relative differences within  $\pm 15\%$ ).

However, the degree of consistency between MIPAS and other measurements is largely affected by their temporal and spatial coincidence. The temporal and spatial coincidence error and the horizontal smoothing error are not taken into account in our error budget. Both errors become large when the spatial variability of target molecule is high. The standard deviations of 5–13% between MIPAS and ground-based FTIR are larger than the estimated measurement uncertainty. For the 2003 MIPAS/ENVISAT and MIPAS-B March measurements differences of 1 to 3 ppbv between 22 and 26 km

**Table 8.** Overview of HNO<sub>3</sub> profile comparisons between MIPAS and validation instruments for different latitudes, seasons and altitude ranges.

Instrument	Time	Region	MIPAS – Instrument [ppbv]		
			below 100 hPa	100–10 hPa	above 10 hPa
SAFIRE	Autumn	N-midlat	±0.5	–0.5–1.0	
SAFIRE	Spring	N-highlat	±0.5	1.0	
MIPAS-STR	Summer	N-midlat	±0.1	0.3	
MIPAS-STR	Spring	N-highlat	±0.5	–0.5–1.0	
ASUR	Autumn–Spring	Trop		–1.3–0.7	0.5
ASUR	Autumn–Spring	N-midlat		–1.2–0.7	±0.1
ASUR	Autumn–Spring	N-highlat		–0.4	0.1
MIPAS-B	Autumn	N-midlat		–0.5–1.0	–0.5–0.1
MIPAS-B	Spring	N-highlat		±1.0	
MIPAS-B	Summer	N-highlat	±0.5	–0.5–1.0	–0.5–0.3
MkIV	Spring	N-highlat	±1.0	±1.0	
MkIV	Autumn	N-midlat	–0.3	±0.5	±0.5
SPIRALE	Winter	N-highlat	–0.3	–3–1.5	
IBEX	Summer	N-midlat	0.3	–0.9–0.5	0.8
ODIN	Autumn–Winter	N-highlat		–2.5––0.5	–0.5–0.3
ODIN	Autumn–Winter	N-midlat		–2––1	–0.5–0.5
ODIN	Autumn–Winter	S-highlat		–1–0	0–0.5
ILAS-II	Spring–Autumn	N-highlat	–0.1	–0.1–0.5	–0.8–0.1
ILAS-II	Spring–Autumn	N-midlat	–0.3–0	±0.7	–0.9––0.1
ILAS-II	Spring–Autumn	S-highlat	–0.3–0.1	±0.5	–3–0
ACE-FTS	Spring	N-midlat	±0.5	±0.5	–0.4––0.2
ACE-FTS	Spring	N-highlat	±0.1	–0.3–0.5	–0.4––0.1

(~50 and 30 hPa) were observed. For the correlative measurements obtained by balloon-borne SPIRALE, much larger discrepancies, as large as 5 ppbv at the level above 100 hPa, are found when the spatial separation of the correlative profiles increases (600–800 km, PV differences up to 35%). At lower and higher altitudes, MIPAS HNO<sub>3</sub> VMRs appear to be higher than those of the IBEX by up to 50–100%. It was also found that MIPAS/ENVISAT normally tends to be in a very good agreement with MIPAS-STR and only occasionally shows somewhat large differences, mostly in terms of a slight overestimation of the HNO<sub>3</sub> VMR. The latter trend is more pronounced in comparison with SAFIRE-A mean profiles, that are almost constantly lower than MIPAS/ENVISAT HNO<sub>3</sub> values. The observed differences could be explained by the fact that the selected collocated HNO<sub>3</sub> profiles, satisfying the spatial and temporal coincidence criteria, can sample different air masses across a region of strong horizontal (and vertical) gradients.

It is worth noting that the highest deviations in HNO<sub>3</sub> VMR were found below 17 km (~100 hPa), with the MkIV being 1.5 ppbv lower than the MIPAS data. For the December 2002 MkIV and MIPAS measurements, substantial differences as large as 2 to 4 ppbv, were observed. From comparisons with MIPAS/ENVISAT ozone retrievals showing similar profile instabilities at the same locations, we conclude

that at least part of the deviations with respect to the MkIV observations have been caused by undetected polar stratospheric clouds leading to oscillations in the MIPAS HNO<sub>3</sub> profiles. A more stringent cloud detection as in case of the IMK-IAA HNO<sub>3</sub> dataset (Wang et al., 2007) would likely have avoided this problem. We therefore conclude that for cases of possible cloud interference (like wintertime polar vortex studies) care must be taken that profiles affected by clouds are sorted out.

Statistical comparison results of MIPAS ESA HNO<sub>3</sub> VMR with respect to those of the Odin/SMR, ILAS-II, ACE-FTS measurements (Figs. 22 to 24), show generally good agreement. For each pair of the correlative measurements, their mean differences averaged over individual latitude bands or over all available bands are generally smaller than the combined instrument measurement errors throughout the whole altitude range between 10 and 50 km, and thus statistically insignificant. The ESA MIPAS and Odin/SMR V2.0 HNO<sub>3</sub> VMR profiles taken between September 2002 and February 2003 showed reasonable agreement (Fig. 22), with the global mean differences generally less than 1 ppbv at the heights between 20 and 40 km (~67 and 4.5 hPa), and with largest differences of ±2 ppbv only seen around 17 km and 22 km (~100 and 50 hPa) at high latitudes of 60°. Much better agreements are observed for the mean HNO<sub>3</sub> VMR profiles

of the ESA MIPAS, with respect to ILAS-II and ACE-FTS measurements (Figs. 23 to 24). The mean differences of the MIPAS ESA data with respect to the ILAS-II data are less than  $\pm 0.5$  ppbv between 10 and 45 km ( $\sim 260$  and  $2.3$  hPa) and the standard deviations  $1$ – $2$  ppbv. The mean differences between MIPAS and ACE-FTS are less than  $\pm 0.1$  to  $0.5$  ppbv and rms deviations are of  $\sim 0.6$  to  $1$  ppbv, with the small values corresponding to the lower and higher altitudes around 10 and 35 km ( $\sim 260$  and  $9$  hPa). The relative differences are 5 to 10% below 30 km ( $\sim 17$  hPa), and 10 to 15% at higher altitudes around 35 km ( $\sim 9$  hPa).

An overall assessment of the MIPAS ESA  $\text{HNO}_3$  inter-comparisons with independent observations – as a function of latitudes, seasons, and altitude ranges and ignoring cases where differences are probably caused by strong atmospheric gradients and presence of clouds – is given in Table 8. Most of these comparisons show that the ESA MIPAS  $\text{HNO}_3$  product is generally in good shape, suggesting suitability of the MIPAS  $\text{HNO}_3$  VMR profiles for use in geophysical studies.

*Acknowledgements.* The FTIR work was supported partly by ESA-funded projects EQUAL and TASTE, and by the ProDEX project CINAMON. The FTIR teams acknowledge their national authorities for supporting the observations and the people who have participated to them. The Belgian teams wish to thank the Stiftungsrat of the Jungfraujoch for supporting the facilities allowing to perform long term and regular observations at that site. Financial support by the DLR (Project 50EE0020) and ESA for the MIPAS-B2 balloon flights is gratefully acknowledged. We thank the Centre National d'Etudes Spatiales (CNES) balloon launching team and the Swedish Space Corporation (SSC) Esrange people for excellent balloon operations and the Free University of Berlin (K. Grunow and B. Naujokat) for meteorological support. The SPIRALE technical team (C. Robert, M. Chartier, L. Pomathiod, T. Lemaire) is acknowledged for making the flights possible and successful. The campaigns were funded by the European Space Agency (ESA), the French Space Agency (CNES). The MIPAS-B and SPIRALE balloon teams thank the Centre National d'Etudes Spatiales (CNES) launching team and the Swedish Space Corporation (SSC) team at Esrange for the success of the validation campaigns. A. Hauchecorne is acknowledged for supplying us with the ECMWF data necessary for the computation of PV as well as F. Coquelet for PV analysis and trajectory calculations. We also thank the Free University of Berlin (K. Grunow and B. Naujokat) for meteorological support. The ASUR team acknowledge the help and support from their colleagues H. Bremer, K. Küllmann, M. Sinnhuber, J. Notholt and K. Künzi prior to and during the measurement campaigns. Odin is a Swedish led satellite project funded jointly by Sweden (SNSB), Canada (CSA), Finland (TEKES) and France (CNES). The ACE mission is supported by the Canadian Space Agency and the Natural Sciences and Engineering Research Council of Canada.

Edited by: P. Hartogh

## References

- Abrams, M. C., Chang, A. Y., Gunson, M. R., Abbas, M. M., Goldman, A., Irion, F. W., Michelsen, H. A., Newchurch, M. J., Rinsland, C. P., Stiller, G. P., and Zander, R.: On the assessment and uncertainty of atmospheric trace gas burden measurements with high resolution infrared solar occultation spectra from space by the ATMOS experiment, *Geophys. Res. Lett.*, 23(17), 2337–2340, doi:10.1029/96GL01794, 1996.
- Austin, J., Garcia, R. R., Russell III, J. M., Solomon, S., and Tuck, A. F.: On the atmospheric photochemistry of nitric acid, *J. Geophys. Res.*, 91(D5), 5477–5485, 1986.
- Bernath, P. F., McElroy, C. T., Abrams, M. C., et al.: Atmospheric Chemistry Experiment (ACE): Mission Overview, *Geophys. Res. Lett.*, 32, L15S01, doi:10.1029/2005GL022386, 2005.
- Bianchini, G., Cortesi, U., Palchetti, L., and Pascale, E.: SAFIRE-A (Spectroscopy of the Atmosphere by Far-Infrared Emission – Airborne): Optimized Instrument Configuration and New Assessment of Improved Performance, *Appl. Optics*, 43(14), 2962–2977, 2004.
- Bianchini, G., Boscaleri, A., Carli, B., Mencaraglia, F., Palchetti, L., and Pascale, E.: Infrared Balloon Experiment: improved instrumental configuration and assessment of instrument performance, *Appl. Optics*, 45, 1041–1051, 2006.
- Boone, C. D., Nassar, R., Walker, K. A., Rochon, Y., McLeod, S. D., Rinsland, C. P., and Bernath, P. F.: Retrievals for the atmospheric chemistry experiment Fouriertransform spectrometer, *Appl. Optics*, 44(33), 7218–7231, 2005.
- Böhringer, H., Fahey, D. W., Fehsenfeld, F. C., and Ferguson, E. E.: The role of ion–molecule reactions in the conversion of  $\text{N}_2\text{O}_5$  to  $\text{HNO}_3$  in the stratosphere, *Planet. Space. Sci.*, 31, 185–191, 1983.
- Bremer, H., von König, M., Kleinböhl, A., Küllmann, H., Künzi, K., Bramstedt, K., Burrows, J. P., Eichmann, K. U., Weber, M., and Goede, A. P. H.: Ozone depletion observed by the Airborne Submillimeter Radiometer (ASUR) during the Arctic Winter 1999/2000, *J. Geophys. Res.*, 107(D20), 8277, doi:10.1029/2001JD000546, 2002.
- Carli, B., Alpaslan, D., Carlotti, M., et al.: First results of MIPAS/ENVISAT with operational Level 2 code, *Adv. Space Res.*, 33, 1012–1019, 2004.
- Carlotti, M.: Global-fit approach to the analysis of limb-scanning atmospheric measurements, *Appl. Optics*, 27, 3250–3254, 1988.
- Cortesi, U., Blom, C. E., Camy-Peyret, C., Chance, K., Davies, J., Goutail, F., Kuttippurath, J., McElroy, C. T., Mencaraglia, F., Oelhaf, H., Petritoli, A., Pirre, M., Pommereau, J. P., Ravegnani, F., Renard, J. B., and Strong, K.: MIPAS ozone validation by stratospheric balloon and aircraft measurements, ESA SP-562, Proceedings Second Atmospheric Chemistry Validation of ENVISAT Workshop (ACVE-2), ESRIN, Frascati, Italy, 2004.
- Cortesi, U., Lambert, J. C., De Clercq, C., et al.: Geophysical validation of MIPAS-ENVISAT operational ozone data, *Atmos. Chem. Phys. Discuss.*, 7, 5805–5939, 2007, <http://www.atmos-chem-phys-discuss.net/7/5805/2007/>.
- de Zafra, R. L. and Smyshlyayev, S. P.: On the formation of  $\text{HNO}_3$  in the Antarctic mid to upper stratosphere in winter, *J. Geophys. Res.*, 106(D19), 23 115–23 126, doi:10.1029/2000JD000314, 2001.
- Dragani, R., Redaelli, G., Mariotti, A., Rudakov, V. V., MacKenzie, A. R., Stefanutti, L., and Visconti, G.: High resolution strato-

- spheric tracer fields reconstructed with Lagrangian techniques: a comparative analysis of predictive skill, *J. Atmos. Sci.*, 59, 1943–1958, 2002.
- Dudhia, A., Jay, V. L., and Rodgers, C. D.: Microwindow selection for high-spectral-resolution sounders, *Appl. Optics*, 41(18), 3665–3673, 2002.
- ESA, Envisat: MIPAS, An instrument for atmospheric chemistry and climate research, ESA SP-1229, European Space Agency, Noordwijk, The Netherlands, 2000.
- Fischer, H. and Oelhaf, H.: Remote sensing of vertical profiles of atmospheric trace constituents with MIPAS limb emission spectrometers, *Appl. Optics*, 35(16), 2787–2796, 1996.
- Fix, A., Ehret, G., Flentje, H., Poberaj, G., Gottwald, M., Finkenzeller, H., Bremer, H., Bruns, M., Burrows, J. P., Kleinböhl, A., Küllmann, H., Kuttippurath, J., Richter, A., Wang, P., Heue, K.-P., Platt, U., and Wagner, T.: SCIAMACHY validation by aircraft remote measurements: Design, execution, and first results of the SCIA-VALUE mission, *Atmos. Chem. Phys.*, 5, 1273–1289, 2005, <http://www.atmos-chem-phys.net/5/1273/2005/>.
- Flaud, J. M., Perrin, A., Orphal, J., Kou, Q., Flaud, P.-M., Dutkiewicz, Z., and Piccolo, C.: New analysis of the  $\nu_5 + \nu_9 - \nu_9$  hot band of  $\text{HNO}_3$ , *J. Quant. Spectrosc. Ra.*, 77, 355–364, 2003.
- Friedl-Vallon, F., Maucher, G., Kleinert, A., Lengel, A., Keim, C., Oelhaf, H., Fischer, H., Seefeldner, M., and Trieschmann, O.: Design and characterization of the balloon-borne Michelson Interferometer for Passive Atmospheric Sounding (MIPAS-B2), *Appl. Optics*, 43, 3335–3355, 2004.
- Gille, J. C. and Russell, J. M.: The Limb Infrared Monitor of the Stratosphere: Experiment Description, Performance, and Results, *J. Geophys. Res.*, 89, 5125–5140, 1984.
- Glatthor, N., von Clarmann, T., Fischer, H., Funke, B., Gil-López, S., Grabowski, U., Höpfner, M., Kellmann, S., Linden, A., López-Puertas, M., Mengistu Tsidu, G., Milz, M., Steck, T., Stiller, G. P., and Wang, D. Y.: Retrieval of stratospheric ozone profiles from MIPAS/ENVISAT limb emission spectra: a sensitivity study, *Atmos. Chem. Phys.*, 6, 2767–2781, 2006, <http://www.atmos-chem-phys.net/6/2767/2006/>.
- Gunson, M. R., Abbas, M. M., Abrams, M. C., Allen, M., Brown, L. R., Brown, T. L., Chang, A. Y., Goldman, A., Irion, F. W., Lowes, L. L., Mahieu, E., Manney, G. L., Michelsen, H. A., Newchurch, M. J., Rinsland, C. P., Salawitch, R. J., Stiller, G. P., Toon, G. C., Yung, Y. L., and Zander, R.: The Atmospheric Trace Molecule Spectroscopy (ATMOS) experiment: Deployment on the ATLAS Space Shuttle missions, *Geophys. Res. Lett.*, 23(17), 2333–2336, doi:10.1029/96GL01569, 1996.
- Hase, F.: Inversion von Spurengasprofilen aus hochaufgelösten bodengebundenen FTIR-Messungen in Absorption, Dissertation, FZK Report No. 6512, Forschungszentrum Karlsruhe, Germany, 2000.
- Hase, F., Hannigan, J. W., Coffey, M. T., et al.: Intercomparison of retrieval codes used for the analysis of high-resolution, ground-based FTIR measurements, *J. Quant. Spectrosc. Ra.*, 87, 25–52, 2004.
- Hauchecorne, A., Godin, S., Marchand, M., Heese, B., and Souprayen, C.: Quantification of the transport of chemical constituents from the polar vortex to midlatitudes in the lower stratosphere using the high-resolution advection model MIMOSA and effective diffusivity, *J. Geophys. Res.*, 107(D20), 8289, doi:10.1029/2001JD000491, 2002.
- Höpfner M., Stiller, G. P., Kuntz, M., et al.: The Karlsruhe optimized and precise radiative transfer algorithm, Part II: Interface to retrieval applications, *SPIE Proceedings*, 3501, 186–195, 1998.
- Höpfner, M., Blom, C. E., Echle, G., Glatthor, N., Hase, F., Stiller, G.: Retrieval simulations for MIPAS-STR measurements, Smith, W. L. [Hrsg.] *IRS 2000: Current Problems in Atmospheric Radiation; Proc. of the Internat. Radiation Symp.*, St. Petersburg, Russia, July 24–29, 2000 Hampton, Va.: DEEPACK Publ., 2001.
- Hübler, G., Fahey, D. W., Kelly, K. K., et al.: Redistribution of reactive odd nitrogen in the lower Arctic stratosphere, *Geophys. Res. Lett.*, 17(4), 453–456, doi:10.1029/90GL00114, 1990.
- Irie, H., Kondo, Y., Koike, M., et al.: Validation of  $\text{NO}_2$  and  $\text{HNO}_3$  measurements from the Improved Limb Atmospheric Spectrometer (ILAS) with the version 5.20 retrieval algorithm, *J. Geophys. Res.*, 107(D24), 8206, doi:10.1029/2001JD001304, 2002.
- Irie, H., Sugita, T., Nakajima, H., et al.: Validation of stratospheric nitric acid profiles observed by Improved Limb Atmospheric Spectrometer (ILAS)-II, *J. Geophys. Res.*, 111, D11S03, doi:10.1029/2005JD006115, 2006.
- Irion, F. W., Gunson, M. R., Toon, G. C., et al.: Atmospheric Trace Molecule Spectroscopy (ATMOS) Experiment Version 3 data retrievals, *Appl. Optics*, 41(33), 6968–6979, 2002.
- Kawa, S. R., Fahey, D. W., Anderson, L. C., Loewenstein, M., and Chan, K. R.: Measurements of total reactive nitrogen during the Airborne Arctic Stratospheric Expedition, *Geophys. Res. Lett.*, 17(4), 485–488, doi:10.1029/89GL03711, 1990.
- Keim, C., Blom, C. E., Von Der Gathen, P., Gulde, T., Höpfner, M., Liu, G. Y., Oulanovski, A., Piesch, C., Ravegnani, F., Sartorius, C., Schlager, H., and Volk, C. M.: Validation of MIPAS-ENVISAT by correlative measurements of MIPAS-STR, *Proc. ACVE-2 meeting*, 3–7 May 2004, Frascati, Italy, ESA SP-562, 2004.
- Kiefer, M., von Clarmann, T., Grabowski, U., De Laurentis, M., Mantovani, R., Milz, M., and Ridolfi, M.: Characterization of MIPAS elevation pointing, *Atmos. Chem. Phys.*, 7, 1615–1628, 2007, <http://www.atmos-chem-phys.net/7/1615/2007/>.
- Kleinböhl, A., Bremer, H., von König, M., Küllmann, H., Künzi, K., Goede, A. P. H., Browell, E. V., Grant, W. B., Toon, G. C., Blumenstock, T., Galle, B., Sinnhuber, B.-M., and Davies, S.: Vortexwide denitrification of the Arctic polar stratosphere in winter 1999/2000 determined by remote observations, *J. Geophys. Res.*, 108(D5), 8305, doi:10.1029/2001JD001042, 2003.
- Kleinböhl, A., Kuttippurath, J., Sinnhuber, M., Sinnhuber, B.-M., Küllmann, H., Künzi, K., and Notholt, J.: Rapid meridional transport of tropical airmasses to the Arctic during the major stratospheric warming in January 2003, *Atmos. Phys. Chem.*, 5, 1291–1299, 2005.
- Koike, M., Kondo, Y., Irie, H., et al.: A comparison of Arctic  $\text{HNO}_3$  profiles measured by the Improved Limb Atmospheric Spectrometer and balloon-borne sensors, *J. Geophys. Res.*, 105(D5), 6761–6771, 2000.
- Kumer, J. B., Mergenthaler, J. L., Roche, A. E., Nightingale, R. W., Ely, G. A., Uplinger, W. G., Gille, J. C., Massie, S. T., Bailey, P. L., Gunson, M. R., Abrams, M. C., Toon, G. C., Sen, B., Blavier, J., Stachnik, R. A., Webster, C. R., May, R. D., Murcray, D. G., Murcray, F. J., Goldman, A., Traub, W. A., Jucks,

- K. W., and Johnson, D. G.: Comparison of correlative data with HNO<sub>3</sub> version 7 from the CLAES instrument deployed on the NASA Upper Atmosphere Research Satellite, *J. Geophys. Res.*, 101(D6), 9621–9656, doi:10.1029/95JD03759, 1996.
- Kuttippurath, J.: Study of stratospheric composition using airborne submillimeter radiometry and a chemical transport model, Ph D. Thesis, ISBN 3-8325-11069-9, Logos Verlag, Berlin, 2005.
- Mees, J., Crewell, S., Nett, H., de Lange, G., van de Stadt, H., Kuipers, J. J., and Panhuysen, R. A.: ASUR – An Airborne SIS-Receiver for Atmospheric Measurements at 625 to 720 GHz, *IEEE Trans. Microwave Theory Tech.*, 43(11), 2543–2548, 1995.
- Mencaraglia, F., Bianchini, G., Boscaleri, A., Carli, B., Ceccherini, S., Raspollini, P., Perrin, A., and Flaud, J.-M.: Validation of MIPAS satellite measurements of HNO<sub>3</sub> using comparison of rotational and vibrational spectroscopy, *J. Geophys. Res.*, 111, D19305, doi:10.1029/2005JD006099, 2006.
- Mengistu Tsidu, G., Stiller, G. P., von Clarmann, T., Funke, B., Höpfner, M., Fischer, H., Glatthor, N., Grabowski, U., Kellmann, S., Kiefer, M., Linden, A., López-Puertas, M., Milz, M., Steck, T., and Wang, D.-Y.: NO<sub>y</sub> from Michelson Interferometer for Passive Atmospheric Sounding on environmental satellite during the southern hemisphere polar vortex split in September/October 2002, *J. Geophys. Res.*, 110(D11), D11301, doi:10.1029/2004JD005322, 2005.
- Moreau, G., Robert, C., Catoire, V., Chartier, M., Camy-Peyret, C., Huret, N., Pirre, M., Pomathiod, L., and Chalumeau, G.: SPIRALE: a multispecies in situ balloon-borne instrument with six tunable diode laser spectrometers, *Appl. Optics*, 44, 28, 5972–5989, 2005.
- Murtagh, D. P., Frisk, U., Merino, F., et al.: An overview of the Odin atmospheric mission, *Can. J. Phy.*, 80(4), 309–319, 2002.
- Oelhaf, H., Blumenstock, T., de Mazière, M., Mikuteit, S., Vigouroux, C., Wood, S., Bianchini, G., Baumann, R., Blom, C., Cortesi, U., Liu, G. Y., Schlager, H., Camy-Peyret, C., Catoire, V., Pirre, M., Strong, K., and Wetzell, G.: Validation of MIPAS-ENVISAT Version 4.61 HNO<sub>3</sub> operational data by stratospheric balloon, aircraft and ground-based measurements, in: Proceedings of the Second Workshop on the Atmospheric Chemistry Validation of ENVISAT (ACVE-2), 3–7 May 2004, ESA-ESRIN, Frascati, Italy, edited by: Danesy, D., vol. ESA SP-562, CD-ROM, ESA Publications Division, ESTEC, Postbus 299, 2200 AG Noordwijk, The Netherlands, August 2004.
- Piesch, C., Gulde, T., Sartorius, C., Friedl-Vallon, F., Seefeldner, M., Wölfel, M., Blom, C.E., and Fischer, H.: Design of a MIPAS instrument for high-altitude aircraft, *Proc. of the 2nd Internat. Airborne Remote Sensing Conference and Exhibition, ERIM, Ann Arbor, MI, Vol. II*, 199–208, 1996.
- Pougatchev, N. S. and Rinsland, C. P.: Spectroscopic study of the seasonal variation of carbon monoxide vertical distribution above Kitt Peak, *J. Geophys. Res.*, 100, 1409–1416, 1995.
- Pougatchev, N. S., Connor, B. J., and Rinsland, C. P.: Infrared measurements of the ozone vertical distribution above Kitt Peak, *J. Geophys. Res.*, 100, 16 689–16 697, 1995.
- Raspollini, P., Belotti, C., Burgess, A., et al.: MIPAS level 2 operational analysis, *Atmos. Chem. Phys.*, 6, 5605–5630, 2006, <http://www.atmos-chem-phys.net/6/5605/2006/>.
- Redaelli, G.: Lagrangian techniques for the analysis of stratospheric measurements, Ph.D thesis, University of L'Aquila, Italy, 1997.
- Ridolfi, M., Carli, B., Carlotti, M., von Clarmann, T., Dinelli, B., Dudhia, A., Flaud, J.-M., Höpfner, M., Morris, P. E., Raspollini, P., Stiller, G., and Wells, R. J.: Optimized forward and retrieval scheme for MIPAS near-real-time data processing, *Appl. Optics*, 39(8), 1323–1340, 2000.
- Riese, M., Tie, X., Brasseur, G., Offermann, D., and Spang, R.: Three-dimensional model simulations of CRISTA trace gas measurements, *Adv. Space Res.*, 26/6, 971–974, doi:10.1016/S0273-1177(00)00039-9, 2000.
- Rinsland, C. P., Jones, N. B., Connor, B. J., et al.: Northern and southern hemisphere ground-based infrared measurements of tropospheric carbon monoxide and ethane, *J. Geophys. Res.*, 103, 28 197–28 217, 1998.
- Rodgers, C. D.: Retrieval of atmospheric temperature and composition from remote measurements of thermal radiation, *Rev. Geophys.*, 14, 609–624, 1976.
- Rodgers, C. D.: Characterization and error analysis of profiles retrieved from remote sounding measurements, *J. Geophys. Res.*, 95, 5587–5595, 1990.
- Rodgers, C. D.: Inverse methods for atmospheric sounding: Theory and Practice, Series on Atmospheric, Oceanic and Planetary Physics – Vol. 2, World Scientific Publishing Co., Singapore, 65–100, 2000.
- Rodgers, C. D. and Connor, B. J.: Intercomparison of remote sounding instruments, *J. Geophys. Res.*, 108(D3), 4116, doi:10.1029/2002JD002299, 2003.
- Rothman, L. S., Jacquemart, D., Barbe, A., et al.: The HITRAN 2004 molecular spectroscopic database, *J. Quant. Spectrosc. Ra.*, 96, 139–204, 2005.
- Rothman, L. S., Barbe, A., Benner, D. C., et al.: The HITRAN molecular spectroscopic database: edition of 2000 including updates through 2001, *J. Quant. Spectrosc. Ra.*, 82, 5–44, 2003.
- Santee, M. L., Manney, G. L., Froidevaux, L., Read, W. G., and Waters, J. W.: Six years of UARS Microwave Limb Sounder HNO<sub>3</sub> observations: Seasonal, 23 interhemispheric, and inter-annual variations in the lower stratosphere, *J. Geophys. Res.*, 104(D7), 8225–8246, 1999.
- Santee, M. L., Manney, G. L., Livesey, N. J., and Read, W. G.: Three-dimensional structure and evolution of stratospheric HNO<sub>3</sub> based on UARS Microwave Limb Sounder measurements, *J. Geophys. Res.*, 109, D15306, doi:10.1029/2004JD004578, 2004.
- Santee, M. L., Manney, G. L., Livesey, N. J., Froidevaux, L., MacKenzie, I. A., Pumphrey, H. C., Read, W. G., Schwartz, M. J., Waters, J. W., and Harwood, R. S.: Polar processing and development of the 2004 Antarctic ozone hole: First results from MLS on Aura, *Geophys. Res. Lett.*, 32, L12817, doi:10.1029/2005GL022582, 2005.
- Spang, R., Remedios, J. J., and Barkley, M. P.: Colour indices for the detection and differentiation of cloud types in infra-red limb emission spectra, *Adv. Space Res.*, 33, 1041–1047, 2004.
- Stiller, G. P., Mengistu Tsidu, G., von Clarmann, T., Glatthor, N., Höpfner, M., Kellmann, S., Linden, A., Ruhnke, R., and Fischer, H.: An enhanced HNO<sub>3</sub> second maximum in the Antarctic mid-winter upper stratosphere 2003, *J. Geophys. Res.*, 110, D20303, doi:10.1029/2005JD006011, 2005.
- Sugita, T., Yokota, T., Nakajima, H., Kobayashi, H., Saitoh, N., Kawasaki, H., Usami, M., Saeki, H., Horikawa, M., and Sasano, Y.: A comparative study of stratospheric temperatures between ILAS-II and other data, *SPIE*, 5652, 279–289, 2004.

- Taddei, A., Redaelli, G., Grassi, B., and Visconti, G.: Self-consistency analysis of MIPAS data using the Trajectory Hunting Technique (THT), Proceedings of the Atmospheric Science Conference, 8–12 May 2006, 1830 ESA-ESRIN, Frascati, Italy, 2006.
- Toon, G. C.: The JPL MkIV Interferometer, *Opt. Photonics News*, 2, 19–21, 1991.
- Urban, J., Lautié, N., Le Flochmoën, E., Jiménez, C., Eriksson, P., de La Noë, J., Dupuy, E., Ekström, M., El Amraoui, L., Frisk, U., Murtagh, D., Olberg, M., and Ricaud, P.: Odin/SMR limb observations of stratospheric trace gases: Level 2 processing of ClO, N<sub>2</sub>O, HNO<sub>3</sub>, and O<sub>3</sub>, *J. Geophys. Res.*, 110, D14307, doi:10.1029/2004JD005741, 2005.
- Urban, J., Murtagh, D., Lautié, N., Barret, B., Dupuy, E., de La Noë, J., Eriksson, P., Frisk, U., Jones, A., Le Flochmoën, E., Olberg, M., Piccolo, C., Ricaud, P., and Rösevall, J.: Odin/SMR Limb Observations of Trace Gases in the Polar Lower Stratosphere during 2004–2005, Proc. ESA First Atmospheric Science Conference, 8–12 May 2006, Frascati, Italy, edited by: Lacoste, H., European Space Agency publications, ESA-SP-628, ISBN-92-9092-939-1, ISSN-1609-042X, [http://earth.esrin.esa.it/workshops/atmos2006/participants/68/paper\\_frascati2006.pdf](http://earth.esrin.esa.it/workshops/atmos2006/participants/68/paper_frascati2006.pdf), 2006.
- Vigouroux, C., De Mazière, M., Errera, Q., Chabrilat, S., Mahieu, E., Duchatelet, P., Wood, S., Smale, D., Mikuteit, S., Blumenstock, T., Hase, F., and Jones, N.: Comparisons between ground-based FTIR and MIPAS N<sub>2</sub>O and HNO<sub>3</sub> profiles before and after assimilation in BASCOE, *Atmos. Chem. Phys.*, 7, 377–396, 2007, <http://www.atmos-chem-phys.net/7/377/2007/>.
- von Clarmann, T.: Validation of remotely sensed profiles of atmospheric state variables: strategies and terminology, *Atmos. Chem. Phys.*, 6, 4311–4320, 2006, <http://www.atmos-chem-phys.net/6/4311/2006/>.
- von Clarmann, T., Ceccherini, S., Doicu, A., et al.: A blind test retrieval experiment for limb emission Spectrometry, *J. Geophys. Res.*, 108(D23), 4746, doi:10.1029/2003JD003835, 2003a.
- von Clarmann, T., Glatthor, N., Grabowski, U., et al.: Retrieval of temperature and tangent altitude pointing from limb emission spectra recorded from space by the Michelson interferometer for passive atmosphere (MIPAS), *J. Geophys. Res.*, 108(D23), 4736, doi:10.1029/2003JD003602, 2003b.
- von König, M., Bremer, H., Eyring, V., Goede, A., Hetzheim, H., Kleipool, Q., Küllmann, H., and Künzi, K.: An airborne submm radiometer for the observation of stratospheric trace gases: Microwave Radiometry and Remote Sensing of the Earth's Surface and Atmosphere, edited by: Pampaloni, P. and Paloscia, S., VSP Utrecht, 409–415, 2000.
- von König, M., Bremer, H., Kleinböhl, A., Küllmann, H., Künzi, K., Goede, A. P. H., Browell, E. V., Grant, W. B., Burris, J. F., McGee, T. G., and Twigg, L.: Using gas-phase nitric acid as an indicator of PSC composition, *J. Geophys. Res.*, 107(D20), 8265, doi:10.1029/2001JD001041, 2002.
- Wang, D. Y., Höpfner, H., Mengistu Tsidu, G., et al.: Validation of nitric acid retrieved by the IMK-IAA processor from MIPAS/ENVISAT measurements, *Atmos. Chem. Phys.*, 7, 1–18, 2007, <http://www.atmos-chem-phys.net/7/1/2007/>.
- Wang, D. Y., von Clarmann, T., Fischer, H., et al.: Validation of stratospheric temperatures measured by MIPAS on ENVISAT, *J. Geophys. Res.*, 110, D08301, doi:10.1029/2004JD5342, 2005.
- Wetzel, G., Oelhaf, H., Friedl-Vallon, F., Kleinert, A., Lengel, A., Maucher, G., Nordmeyer, H., Ruhnke, R., Nakajima, H., Sasano, Y., Sugita, T., and Yokota, T.: Intercomparison and validation of ILAS-II version 1.4 target parameters with MIPAS-B measurements, *J. Geophys. Res.*, 111, D11S06, doi:10.1029/2005JD006287, 2006.
- Wetzel, G., Bracher, A., Funke, B., et al.: Validation of MIPAS-ENVISAT NO<sub>2</sub> operational data, *Atmos. Chem. Phys.*, 7, 3261–3284, 2007, <http://www.atmos-chem-phys.net/7/3261/2007/>.
- World Meteorological Organization: Scientific assessment of ozone depletion: 2002, *Global Ozone Res. and Monit. Proj. Rep. No.*, 47, Geneva, 2003.
- Yamamori, M., Kagawa, A., Kasai, Y., Mizutani, K., Murayama, Y., Sugita, T., Irie, H., and Nakajima, H.: Validation of ILAS-II version 1.4 O<sub>3</sub>, HNO<sub>3</sub>, and temperature data through comparison with ozonesonde, ground-based FTS, and lidar measurements in Alaska, *J. Geophys. Res.*, 111(D11), D11S08, doi:10.1029/2005JD006438, 2006.
- Yokota, T., Nakajima, H., Sugita, T., Tsubaki, H., Ito, Y., Kaji, M., Suzuki, M., Kanzawa, H., Park, J. H., and Sasano, Y.: Improved Limb Atmospheric Spectrometer (ILAS) data retrieval algorithm for version 5.20 gas profile products, *J. Geophys. Res.*, 107(D24), 8216, doi:10.1029/2001JD000628, 2002.